HHS Public Access

Author manuscript

Nature. Author manuscript; available in PMC 2017 May 30.

Published in final edited form as:

Nature. 2016 December 15; 540(7633): 428–432. doi:10.1038/nature20603.

Epigenetic stress responses induce muscle stem cell aging by *Hoxa9* developmental signals

Simon Schwoerer[1], **Friedrich Becker**[1], **Christian Feller**[2], **Ali H. Baig**[1], **Ute Koeber**[1], **Henriette Henze**[1], **Johann M. Kraus**[3], **Beibei Xin**[4], **André Lechel**[5], **Daniel B. Lipka**[6], **Christy S. Varghese**[1], **Manuel Schmidt**[1], **Remo Rohs**[4], **Ruedi Aebersold**[2,7], **Kay L. Medina**[8], **Hans A. Kestler**[1,3], **Francesco Neri**[1], **Julia von Maltzahn**[1,10], **Stefan Tuempel**[1,10], and **K. Lenhard Rudolph**[1,9,10]

[1]Fritz-Lipmann-Institute – Leibniz-Institute on Aging, Beutenbergstrasse 11, 07745 Jena, Germany [2]Department of Biology, Institute of Molecular Systems Biology, ETH Zürich, Auguste-Piccard-Hof 1, 8093 Zürich, Switzerland [3]Institute of Medical Systems Biology, Ulm University, James-Franck-Ring, 89081 Ulm, Germany [4]Molecular and Computational Biology Program, University of Southern California, 1050 Childs Way, Los Angeles, CA 90089, USA [5]Department of Internal Medicine I, Ulm University, Albert-Einstein-Allee 23, 89081 Ulm, Germany [6]Division of Epigenomics and Cancer Risk Factors, DKFZ, Im Neuenheimer Feld 280, 69120 Heidelberg, Germany [7]Faculty of Science, University of Zürich, Zürich, Switzerland [8]Department of Immunology, Mayo Clinic, 200 First Street SW, Rochester, MN 55905, USA [9]Faculty of Medicine, Friedrich-Schiller-University, Jena, Germany

SUMMARY

The functionality of stem cells declines during aging thereby contributing to aging-associated impairments in tissue regeneration and function[1]. Alterations in developmental pathways have been associated with declines in stem cell function during aging[2–6] but the nature of this process remains poorly defined. *Hox* genes are key regulators of stem cells and tissue patterning during

[10]Correspondence should be addressed to K.L.R., S.T. and J.V.M., Tel: ++49-3641-656350, Fax: ++49-3641-656351, lenhard.rudolph@leibniz-fli.de, stefan.tuempel@leibniz-fli.de, julia.vonmaltzahn@leibniz-fli.de.

AUTHOR CONTRIBUTIONS

S.S. designed and performed the majority of experiments, analyzed data, interpreted results and wrote the manuscript. F.B. designed and performed ChIP and FISH experiments, analyzed data, interpreted results and wrote the manuscript. C.F. and R.A. designed and performed LC-MS experiments, analyzed data, interpreted results and wrote the manuscript. A.H.B., U.K., H.H., C.S.V. and M.S. performed individual experiments and analyzed data. A.L. performed microarray experiment. D.B.L. provided support and suggestions for ChIP experiments. K.L.M. provided *Hoxa9*$^{-/-}$ mice. J.M.K. and H.A.K. performed microarray and pathway analysis, analyzed putative Hoxa9 binding sites and provided support for statistical analysis. B.X. and R.R. conducted analysis of putative Hoxa9 binding sites. F.N. analyzed RNA-sequencing data and performed correlation analysis. J.V.M. and S.T. conceived the project, designed and performed experiments, interpreted results and wrote the manuscript. K.L.R. conceived the project, designed experiments, interpreted results and wrote the manuscript.

DATA AVAILABILITY STATEMENT

Microarray and RNA-sequencing data that support the findings of this study have been deposited in GEO with the accession code GSE87812. Further data that support the findings of this study are available from the corresponding authors upon reasonable request. Source data for Figures and Extended Data Figures are provided with the paper.

The authors declare no conflict of interest.

embryogenesis with an unknown role in aging[7,8]. This study identifies an altered epigenetic stress response in muscle stem cells (also known as satellite cells = SCs) of aged compared to young mice. This includes aberrant global and site-specific induction of active chromatin marks in activated SCs from aged mice resulting in the specific induction of *Hoxa9* among all *Hox* genes. Hoxa9 in turn activates several developmental pathways and represents a decisive factor separating gene expression of SCs from aged compared to young mice. This includes most of the currently known inhibitors of SC function in aging muscle such as Wnt-, TGFß-, JAK/STAT- and senescence signaling[2–4,6]. Inhibition of aberrant chromatin activation or deletion of *Hoxa9* suffices to improve SC function and muscle regeneration in aged mice, while overexpression of *Hoxa9* mimics aging-associated defects in SCs from young mice, which can be rescued by inhibition of Hoxa9-targeted developmental pathways. Together, these data delineate an altered epigenetic stress response in activated SCs from aged mice, which limits SC function and muscle regeneration by Hoxa9-dependent activation of developmental pathways.

Keywords

Skeletal muscle; satellite cell; regeneration; stem cells; aging; *Hox* genes; development; histone modifications; chromatin systems biology

Age-dependent decline in the number and function of $Pax7^+$ SCs impair the regenerative capacity of skeletal muscle[2,4,9] and pathways that contribute to this process[2–6] include several genes and pathways that regulate embryonic development[10–13]. Despite these parallels the function of the master regulators of development, *Hox* genes, has not been determined in SC aging. An analysis of freshly isolated, *in vivo* activated SCs from young adult and aged mice (Extended Data Fig. 1a–e) revealed a specific upregulation of *Hoxa9* in SCs from aged mice, both on mRNA (Fig. 1a, Extended Data Fig. 2a,b) and protein level (Fig. 1b,c). Similar results were obtained by immunofluorescence staining of SCs (Extended Data Fig. 2c) and myofiber-associated SCs (Fig. 1d,e, Extended Data Fig. 2d) that were activated in culture (Extended Data Fig. 1f,g).

Aging reduces the proliferative and self-renewal capacity of SCs in wildtype mice ($Hoxa9^{+/+}$, Extended Data Fig. 3; ref. [2,9,14,15]). Homozygous deletion of *Hoxa9* ($Hoxa9^{-/-}$) did not affect the colony forming capacity of SCs from young adult mice but ameliorated aging-associated impairment in colony formation of single cell-sorted SCs in culture (Fig. 2a). *Hoxa9* deletion also increased the self-renewal of myofiber-associated SCs from aged mice in culture but had no effect on SCs from young adult mice under these conditions (Extended Data Fig. 4a–c). Similar results were obtained by siRNA-mediated knockdown of *Hoxa9* in myofiber-associated SC cultures derived from aged mice (Extended Data Fig. 4d–h). The number of SCs decreases in resting tibialis anterior (TA) muscle of aging wildtype mice, which was not affected by *Hoxa9* gene status (Extended Data Fig. 5a). However, homozygous deletion or siRNA-mediated knockdown of *Hoxa9* increased the total number of $Pax7^+$ SCs (Fig. 2b) and improved myofiber regeneration in injured muscle of aged mice almost to the levels in young adult mice (Fig. 2c, Extended Data Fig. 5b–f), albeit without affecting overall SC proliferation rates 7 days after muscle injury (Extended Data Fig. 5g,h). *Hoxa9* gene deletion also improved the cell-autonomous, *in vivo* regenerative capacity of

transplanted SCs derived from aged donor mice but did not affect the capacity of SCs derived from young adult donors (Fig. 2d,e, Extended Data Fig. 6a). Similarly, *Hoxa9* downregulation by shRNA infection rescued the regenerative capacity and the engraftment of transplanted SCs derived from aged mice almost to the level of SCs from young adult mice (Extended Data Fig. 6b–h). When transduced at similar infection efficiency (Extended Data Fig. 6i), *Hoxa9* shRNA compared to scrambled shRNA improved the self-renewal of serially transplanted SCs from aged mice in primary recipients (Fig. 2f, Extended Data Fig. 6j) as well as the regenerative capacity of 500 re-isolated SCs from primary donors that were transplanted for a second round into the injured TA muscle of secondary recipients (Fig. 2g, Extended Data Fig. 6k). Together, these results demonstrate that the induction of *Hoxa9* limits SC self-renewal and muscle regeneration in aged mice and that the deletion of *Hoxa9* is sufficient to revert these aging-associated deficiencies.

The expression of *Hoxa9* in development and leukemia is actively maintained by Mll1-dependent tri-methylation at lysine 4 of histone 3 (H3K4me3)[16–18]. Chromatin immunoprecipitation (ChIP) revealed that H3K4me3 is strongly enriched at the promoter and first exon of *Hoxa9* in activated SCs from aged compared to young adult mice, which was not detected to the same extent for other *HoxA* genes (Fig. 3a, Extended Data Fig. 7a). ChIPs for Mll1 and Wdr5 (a scaffold protein of the Mll1 complex) revealed increased recruitment of these factors to the *HoxA* cluster with Wdr5 enrichment being defined to the *Hoxa9* locus (Fig. 3b,c). Although no changes were observed for Mll1, both H3K4me3 and Wdr5 showed significantly increased expression in nuclei of myofiber-associated SCs from aged *vs*. young adult mice upon activation (Extended Data Fig. 7b–e). Of note, knockdown of either *Mll1* or *Wdr5* reduced H3K4me3 levels as well as Mll1 recruitment to the *Hoxa9* locus and ameliorated *Hoxa9* induction in activated myofiber-associated SCs from aged mice (Fig. 3d,e, Extended Data Fig. 7f–i). Similar results were obtained by treatment of aged myofiber-associated SCs with OICR-9429, an inhibitor of the Mll1-Wdr5 interaction[19] (Extended Data Fig. 7j,k). Moreover, both *Mll1* knockdown or OICR-9429 treatment increased the self-renewal and lowered the myogenic commitment of myofiber-associated SCs from aged mice (Extended Data Fig. 7l–q) resulting in increased SC numbers in cultures of purified SCs or myofibers derived from aged mice (Extended Data Fig. 7r,s). Importantly, Mll1 inhibition by either stable shRNA knockdown (Extended Data Fig. 7t) or OICR-9429 treatment improved the regenerative capacity of SCs from aged mice when transplanted into injured muscle of recipient mice (Fig. 3f–h). Taken together, these experiments demonstrate that the Mll1 complex contributes to *Hoxa9* induction in activated SCs from aged mice resulting in impairment in SC function and muscle regeneration. *Pax7* expression was downregulated in activated SCs of aged mice (Extended Data Fig. 7u–w) and did not correlate with Hoxa9 expression (Extended Data Fig. 7x,y), indicating that Mll1-dependent regulation of Pax7 target genes[20] was not involved in the Mll1-dependent induction of *Hoxa9* in activated SCs from aged mice.

Next, a global analysis of histone post-translational modifications was carried out on freshly isolated SCs harvested before muscle injury (quiescent state) or two, three and five days after *in vivo* SC activation mediated by muscle injury (Fig. 4a,b, Extended Data Fig. 8a). Using a recently developed mass spectrometry-based proteomic strategy[21], 46 histone H3 and H4 lysine acetylation and methylation motifs were quantified. Quiescent SCs from aged

mice compared to young adult mice showed elevated levels of repressive marks (H3K9me2 and H3K27me3; Extended Data Fig. 8a; consistent with ref. [22]) and lower amounts of histone modifications typically enriched on active genes (e.g. various H4 acetylation motifs, H3K14ac, H3K18ac, H3K36me2; Extended Data Fig. 8a). A time-dependent shift towards a heterochromatic state occurred during SC activation in young adult mice, while activation in aged SCs generated the opposite response (Fig. 4a,b). While selective active marks such as H3 and H4 acetylation motifs declined in SCs from young adult mice during activation, there was a substantial increase of these marks in aged SCs (Fig. 4a–c). On the other hand, repressive marks (e.g. H3K27me3) decreased in SCs from aged mice but remained stable in SCs from young adult mice (Fig. 4a,b,d). The observed shift of the chromatin towards a more permissive state upon activation appeared to also affect the *HoxA* cluster as this locus displayed an increased chromatin decompaction upon activation in aged mice but not in young adult mice (Fig. 4e–g).

To analyze the functional contribution of different types of chromatin modifications in activated SCs from aging mice a set of genetic and pharmacologic experiments was conducted. The expression of key enzymes involved in chromatin modifications was similar in activated SCs from young adult and aged mice (Extended Data Fig. 8b). However, knockdown of the acetyltransferases *MOF*, *CBP* or *PCAF* improved the proliferative capacity of SCs from aged mice in bulk culture, whereas knockdown of histone deacetylases led to a reduction (Fig. 4h). Furthermore, knockdown of the H3K27 demethylases *UTX*, *UTY* or *Kdm7a* promoted the proliferation of aged SCs, which was instead inhibited by knockdown of the PRC2 complex members *SUZ12* and *Ezh2* (Fig. 4i), the primary protein complex responsible for H3K27me3. Multi-acetylation motifs, as observed in activated SC from aged mice (Fig. 4b,c), are preferred binding sites for bromodomain-containing proteins[23]. Eight of 11 non-toxic bromodomain inhibitors available from the Structural Genomics Consortium exhibited positive effects on the proliferative capacity of SCs from aged mice (Extended Data Fig. 8c,d, $p=4.2\times10^{-4}$). Targeting major classes of chromatin modifiers by a selected set of siRNAs (Supplementary Table 1) revealed a significant inverse correlation ($r = -0.612$) between siRNA-mediated changes in Hoxa9 protein expression and the proliferative capacity of SCs from aged mice, with no such effects observed in SCs from young adult mice (Fig. 4j,k). Similarly, siRNAs against *MOF* and *UTX* as well as bromodomain inhibitors led to significant decreases of Hoxa9 protein level in activated myofiber-associated SCs from aged mice (Extended Data Fig. 8e–g). In summary, activated SCs from aged mice exhibit site-specific and global aberrations in the epigenetic stress response resulting in *Hoxa9* activation and profound negative effects on SC function, which are ameliorated by targeting the respective enzymes underlying these alterations.

By analyzing the downstream effects of *Hoxa9* induction through lentiviral-mediated *Hoxa9* overexpression, we found a strong reduction in the colony forming and proliferative capacity of SCs from young adult mice (Extended Data Fig. 9a–c). The overexpression of other *Hox* genes exerted similar effects (Extended Data Fig. 9d) but the results on *Hoxa9* are likely of highest relevance for physiological aging since only *Hoxa9* was upregulated in activated SCs from aged mice (Fig. 1). The impaired myogenic capacity of SCs in response to *Hoxa9* overexpression was associated with increased rates of apoptosis and decreased cell proliferation (Extended Data Fig. 9e–h). Furthermore, *Hoxa9* induction associated with the

suppression of several cell cycle regulators and induction of cell cycle inhibitors and senescence-inducing genes (Extended Data Fig. 9i) as well as with elevated staining for senescence-associated β-galactosidase (Extended Data Fig. 9j–k). Microarray expression analysis of *Hoxa9* overexpressing SCs compared to controls revealed that among the top 12 pathways regulated by *Hoxa9* were several major developmental pathways that have previously been shown to impair SC function and muscle regeneration in the context of aging (Fig. 5a, Extended Data Fig. 9l–o; ref. [2,3,5,6,9,24,25]). ChIP analysis of putative Hoxa9 binding sites (Supplementary Table 1) in *Hoxa9* overexpressing primary myoblasts indicated that a high number of these genes are likely direct targets of Hoxa9 (Extended Data Fig. 9p; cumulative p-value over tested genes: $p=1\times10^{-7}$). Hoxa9 strongly induced downstream targets of the Wnt-, TGFß- and JAK/STAT pathways, but targeted activation of each one of these pathways alone only led to slight changes in the expression of target genes of the other two pathways (Extended Data Fig. 9q–s) suggesting that *Hoxa9* acts as a central hub required for the parallel induction of these pathways in aged SCs. Of note, inhibition of *STAT3*, *BMP4* or *ß-Catenin* by shRNAs as well as pharmacological inhibition of these pathways was sufficient to improve the myogenic colony forming capacity of SCs overexpressing *Hoxa9* (Fig. 5b, Extended Data Fig. 10a,b). In line with previous results, knockdown of *STAT3* also increased the total number and lowered early differentiation of myofiber-associated SCs from aged mice, and in addition, increased the regenerative capacity of transplanted SCs from aged mice to a similar extend as *Hoxa9* knockdown (Extended Data Fig. 10c–g).

Differentially expressed genes were determined using RNA-sequencing data of freshly isolated, *in vivo* activated SCs from young adult and aged wildtype mice as well as from aged $Hoxa9^{-/-}$ mice. There was a highly significant overlap between genes induced by *Hoxa9* overexpression in SCs from young adult mice with those genes that were dysregulated in *in vivo* activated SCs from aged compared to young adult mice ($p=2.2\times10^{-19}$, Extended Data Fig. 10h). Pathways that are currently known to be associated with SC aging were again among the highest ranked pathways differentially expressed in activated SCs from aged compared to young adult mice including MAPK-, TGFß-, Wnt- and JAK/STAT-signaling (Fig. 5c). Of note, *Hoxa9* deletion completely abrogated the separate clustering of gene expression profiles of activated SCs from aged compared to young adult mice (Fig. 5d–e). Comparing transcriptomes of activated SC from aged $Hoxa9^{+/+}$ to aged $Hoxa9^{-/-}$ mice re-established the separate clustering (Fig. 5f) characterized by enrichment of the same set of developmental pathways that associate with SC aging in wildtype mice (Fig. 5g, compare to Fig. 5c).

Taken together, the current study provides experimental evidence that an aberrant epigenetic stress response impairs the functionality of SCs from aged mice by *Hoxa9*-dependent activation of developmental signals (Extended Data Fig. 10i). Importantly, a proof of concept is provided that key enzymes that promote global and site-specific alterations in the epigenetic stress response of aged SCs are druggable and that the inhibition of these targets leads to improvement in SC function and muscle regeneration during aging. These findings provide experimental support for the recent hypothesis that a “shadowed” dysregulation of developmental pathways represents a driving force of stem cell and tissue aging[26,27].

METHODS

Data reporting

No statistical methods were used to estimate sample size. No randomization was used. No animals were excluded. The evaluator was blinded to the identity of the specific sample as much as the nature of the experiment allowed it.

Mice

We purchased female young adult C57/BL6j mice (3–4 months) and aged C57/BL6J mice (22–28 months) from Janvier (Wildtype mice). Female and male *Hoxa9*$^{-/-}$ mice have been described[28] and were obtained together with age- and gender-matched littermate controls from Kay L. Medina (Mayo Clinic, Rochester, USA). Mice were housed in a pathogen-free environment and fed with a standard diet *ad libitum*. Animal experiments are approved by the Landesamt für Verbraucherschutz Abteilung Gesundheitlicher und technischer Verbraucherschutz (Germany) under Reg.-Nr. 03-006/13, 03-012/13 and 03-007/15.

Muscle injury

Mice were anaesthetized using isoflurane in air and oxygen through a nose cone. For SC activation, muscles were injured by injecting a total volume of 50 µl of 1.2% $BaCl_2$ (Sigma) into approximately 20 sites in the hindlimb muscles. For regeneration and transplantation experiments, tibialis anterior (TA) muscle of the right leg was injected with 50 µl Cardiotoxin (10 µM, Sigma).

Satellite cell isolation and FACS

Muscles from hindlimbs from young adult or aged mice were dissected and collected in PBS on ice. Muscles were rinsed with PBS, minced with scissors and incubated in DMEM with Collagenase (0.2%, Biochrom) for 90 min at 37°C and 70 rpm. Digested muscles were washed with PBS/10% FBS, triturated and incubated in Collagenase (0.0125%) and Dispase (0.4%, Life Technologies) for 30 min at 37°C and 100 rpm. The muscle slurry was diluted with PBS/10% FBS, filtered through 100 µm cell strainers and spun down at 500 g for 5 min. Cell pellets were resuspended in FACS buffer (HBSS/2% FBS) and filtered through 40 µm cell strainers and pelleted at 500 g for 5 min. Pellets were resuspended in FACS buffer and stained with anti-mouse CD45 PE conjugate (30-F11, eBioscience), anti-mouse CD11b PE conjugate (M1/70, eBioscience), anti-mouse Sca-1 PE conjugate (D7, BioLegend), anti-mouse CD31 PE/Cy7 conjugate (390, BioLegend) and anti-mouse α7-Integrin Alexa Fluor 647 conjugate (R2F2, AbLab) for 20 min at 4°C on a rotating wheel. Cells were washed with FACS buffer. Live cells were identified as calcein blue positive (1:1,000, Invitrogen) and propidium iodide negative (PI, 1 µg/ml, BD Biosciences). SCs were identified as $CD45^{-}Sca\text{-}1^{-}CD11b^{-}CD31^{-}\alpha7\text{-}Integrin^{+}$. Cell sorting was performed on a FACSAriaIII with Diva Software (BD).

Culture of SCs

SCs and SC-derived primary myoblasts were cultured at 37°C, 5% CO_2, 3% O_2 and 95% humidity in growth medium on collagen/laminin coated tissue culture plates for the

indicated time periods. Growth medium was comprised of F10 (Life Technologies) with 20% Horse serum (GE), 1% Penicillin/Streptomycin (Life Technologies) and 5 ng/ml bFGF (Sigma). For coating, tissue culture plates were incubated with 1 mg/ml collagen (Sigma) and 10 mg/ml laminin (Life Technologies) in ddH_2O for at least 1 h at 37°C and allowed to air-dry. For passaging or FACS analysis, cultured cells were incubated with 0.5 % trypsin/PBS for 3 min at 37°C and collected in FACS buffer. Treatment of SCs with Noggin (Prepotech) or DKK1 (Prepotech) was done at 100 ng/ml concentration. SCs and SC-derived primary myoblasts were treated with 1 μM of chemical probes provided by the Structural Genomics Consortium (SGC, http://www.thesgc.org/chemical-probes/epigenetics)[29,30]. OICR-9429 and Bromodomain Inhibitors were originally described in 19,31–39.

Clonal myogenesis assay

Freshly isolated SCs from young adult and aged mice were sorted in growth medium in 96-well plates using the automated cell deposition unit (ACDU) of the FACSAriaIII. After 5d, wells containing myogenic colonies were counted by brightfield microscopy. For clonal analysis of lentivirus transduced SCs, infected ($EGFP^+$ and/or BFP^+) live ($DAPI^-$) cells were as one cell per well in growth medium and wells containing myogenic colonies were counted by fluorescence microscopy (Axio Observer, Zeiss) after 5d. A colony was defined by the presence of at least two cells.

Alamar blue assay

SCs or SC-derived primary myoblasts were seeded at 500 cells per well in growth medium into 96-well plates. After 4d of culture, the viability was measured by adding Alamar Blue (Life Technologies) as 10% of the sample volume. Cells were incubated for 2h at 37°C and fluorescence intensity was measured at an excitation/emission wavelength of 560/590 nm.

BrdU assay

SCs were incubated with 5 μM BrdU (Sigma) in growth medium for 2h. Cells were fixed with 4% PFA, permeabilized with 0.5% Triton X-100 and incubated with 2N HCl/PBS for 30 min at RT. Incorporated BrdU was detected using anti-BrdU (347580, BD Biosciences) and Alexa-594 fluorochrome (Life Technologies) for 1h at RT. Nuclei were counterstained with DAPI/PBS.

TUNEL assay

TUNEL assay was performed using the In Situ Cell Death Detection Kit, Texas Red (Roche) according to the manufacturer's instructions.

Senescence-associated ß-Galactosidase assay

SCs were fixed in 4% PFA and stained with staining solution (5 mM potassium ferricyanide, 5 mM potassium ferrocyanide, 2 mM $MgCl_2$, 150 mM NaCl, 1 mg/ml X-Gal) in citrate/sodium-phosphate buffer (pH 6) overnight at 37°C. Statining solution was removed by rinsing several times with PBS.

Myofiber isolation and culture

Individual myofibers were isolated from the extensor digitorum longus (EDL) muscle as described previously[40,41]. Isolated myofibers were cultured in DMEM containing 20% FBS and 1% chicken embryo extract (Biomol) in dishes coated with Horse Serum. Freshly isolated fibers or fibers cultured for 24–34h and 72h were fixed with 2% PFA and subjected to immunofluorescence analysis. Clusters of SCs were counted on at least 10–15 fibers per replicate. A cluster was defined by the presence of at least three adjacent cells. For quantification of immunofluorescence staining of myofiber-associated quiescent and activated SCs, at least 20 fibers were analyzed per replicate. Treatment of myofiber-associated SCs with chemical probes provided by the Structural Genomics Consortium (SGC) was done 4h after isolation at 1 μM concentration.

siRNA transfection

Transfection of SCs was performed in a reverse manner: SCs were seeded in growth medium into individual wells of a 384-well plate pre-filled with transfection mix. For floating cultures of single myofibers, transfections were performed 4h after isolation in myofiber culture medium. Transfections were done using Lipofectamin RNAiMAX (Life Technologies) according to manufacturer's instructions. For gene knockdown either Silencer Select siRNAs (Life Technologies) or ON-TARGETplus siRNA SMART-pools (Dharmacon) were used. Respective Silencer Select or ON-TARGETplus SMART-pool non-targeting siRNA were used as negative control. siRNA sequences are found in Supplementary Table 1. Transfection efficiency was monitored using a Cy3-labeled control siRNA (Life Technologies). After transfection, FACS-sorted SCs or myofiber-associated SCs were cultured for the indicated time periods and fixed in 2 % PFA/PBS. *In vivo* knockdown experiments were performed as described earlier[41]. siRNA sequences were modified to the Accell self-delivering format (Dharmacon) and 100 μg Accell siRNA were injected into TA muscles 2d after CTX injury. *In vivo* knockdown was evaluated from SCs isolated from injected TA 3d post transfection. Transfected muscles were harvested 5d after siRNA injection, frozen in 10% sucrose/O.C.T. in liquid nitrogen and stored at −80°C.

Lentivirus production and transduction

Lentivirus was produced in Lenti-X cells (Clonetech) after co-transfection of 15 μg shRNA plasmid, 10 μg psPAX2 helper plasmid and 5 μg pMD2.G according to standard procedures[42]. Virus was concentrated by centrifugation for 2.5h at 25,000 rpm and 4°C, and virus pellet was resuspended in sterile PBS. Lentiviral transduction was carried out in growth medium supplemented with 8 μg/ml Polybrene (Sigma).

Plasmids

cDNA was inserted into the SF-LV-cDNA-EGFP plasmid[43]. Primers used for cloning of individual *Hox* cDNAs are listed in Supplementary Table 1. shRNA was inserted into the SF-LV-shRNA-EGFP plasmid using mir30 primers (Supplementary Table 1). shRNA sequences are listed in Supplementary Table 1.

Satellite cell transplantation

SCs were FACS purified and transduced with a lentivirus on Retronectin (Takara) coated 48-well plates[4]. After 8–10h, SCs were harvested by resuspension and washed several times with FACS buffer. For each engraftment, 10,000 SCs were resuspended in 0.9% NaCl and immediately transplanted into TA muscles of adult immunosuppressed mice that had been injured with CTX 2d before. Immunosuppression with FK506 (5 mg/kg body weight, Sigma) was started at the day of injury using osmotic pumps (model 2004, Alzet) and maintained throughout the entire time of engraftment. Engrafted muscles were harvested 3 weeks after transplantation and fixed in 4% PFA for 30 min at RT followed by incubation in 30% sucrose/PBS overnight at 4°C. Fixed muscles were frozen in 10% sucrose/O.C.T. in liquid nitrogen, stored at −80°C.

Immunohistochemistry

Cryosections of 10 μm were cut from frozen muscle using the Microm HM 550. Cryosections were rinsed once with PBS and fixed in 2% PFA in PBS for 5 min at RT. Sections were rinsed three times for 5 min with PBS, permeabilized with 0.5 % Triton X-100/0.1 M Glycine in PBS for 5 min at RT followed again by rinsing them three times with PBS. Sections were blocked in PBS supplemented with 5 % Horse serum and 1:40 Mouse on mouse blocking reagent (Vector labs) for 1 h at RT. Incubation with primary antibodies was carried out overnight at 4°C. The next day, sections were rinsed three times with PBS followed by incubation with secondary antibodies for 1 h at RT. Sections were rinsed again with PBS and nuclei were counterstained with 1:1,000 DAPI/PBS before mounting with Permaflour (Thermo Scientific). Slides were stored at 4°C until analysis. The following primary antibodies were used: 1:1,000 chicken anti-GFP (ab6556, AbCam), 1:1,000 rabbit anti-Laminin (L9393, Sigma), 1:200 rabbit anti-Ki67 (ab15580, AbCam), undiluted mouse anti-Pax7 (DSHB). The following secondary antibodies were used at 1:1,000 concentration: anti-chicken IgG Alexa-Fluor 488, anti-rabbit IgG Alexa-Fluor 488, anti-mouse IgG1 Alexa-Fluor 594 (Life Technologies).

Immunofluorescence

Freshly isolated SCs were allowed to settle on poly-L-lysine coated diagnostic microscope slides for 30 min at RT. All cells and myofibers were fixed with 2% PFA/PBS, permeabilized with 0.5% Triton X-100/PBS and blocked with 10 % Horse Serum/PBS for 1h at RT. Cells and fibers were stained with primary antibodies in blocking solution overnight at 4°C. Samples were washed three times with PBS and incubated with secondary antibodies for 1h at RT. Nuclei were counterstained with DAPI/PBS. Cultured cells were kept in PBS; freshly isolated SCs and myofibers were mounted with Permaflour. The following primary antibodies were used: undiluted mouse anti-Pax7 (DSHB), 1:300 rabbit anti-Hoxa9 (07-178, Millipore), 1:500 mouse anti-MLL1 (05-765, Millipore), 1:500 rabbit anti-WDR5 (A302-429A, Bethyl Laboratories), 1:300 rabbit anti-H3K4me3 (C15410003-50, Diagenode), 1:200 rabbit anti-MyoD (sc-304, Santa Cruz). The following secondary antibodies were used at 1:1,000 concentration: anti-rabbit IgG Alexa-Fluor 488, anti-mouse IgG Alexa-Fluor 594, anti-mouse IgG1 Alexa-Fluor 594 (Life Technologies).

Fluorescence in situ hybridization (FISH)

Chromatin compaction FISH was done as described previously[44]. DNA of the 3′- and 5′ probe (Fosmid clones WIBR1-1312N03 and WIBR1-2209G09, CHORI) was labeled with digoxigenin or biotin by nick-translation (Roche). 100 ng of probe DNA was used per slide, together with 5 μg mouse CotI DNA (Life Technologies) and 5 μg sssDNA (Ambion). 5,000 freshly sorted SCs were allowed to settle on poly-L-lysine coated diagnostic microscope slides for 30 min at RT and were fixed with 2% PFA/PBS for 5 min. After washing three times with PBS, slides were incubated with 0.1M HCl for 5 min and permeabilized with 0.5% Triton in 0.5% Saponin/PBS for 10 min before freeze-thaw in 20% glycerol/PBS. Denaturation was performed in 50% formamide, 1% Tween-20 and 10% Dextran Sulfate/2× SSC for 5 min at 75°C before applying the hybridization cocktail. Probes were hybridized overnight at 37°C in a humified chamber. Slides were rinsed three times with 2× SSC, blocked with 2% BSA in 0.1% Tween-20/PBS for 1h at RT, and hybridized probes were visualized with anti-Digoxigenin-Rhodamine (S7165, Millipore) and Streptavidin-Cy2 (016-220-084, IR USA) for 30 min at RT. Nuclei were counterstained with DAPI.

Digital image acquisition and processing

Immunofluorescence images of muscle sections, myofibers and freshly isolated SCs were acquired using the upright microscope Axio Imager (Zeiss) with 10×, 20× and 100× objectives and a monochrome camera. Brightfield and immunofluorescence images of cultured SCs were captured using the microscope Axio Observer (Zeiss) with 5×, 10× and 20× objectives and a monochrome camera. Image acquisition and processing was performed using the ZEN 2012 software (Zeiss). Brightness and contrast adjustments were applied to the entire image before the region of interest was selected. For the analysis of muscle sections, several images covering the whole area of the section were acquired in a rasterized manner and assembled in Photoshop CS6 (Adobe) to obtain an image of the entire section. Images were analyzed using Image J software. The number of $Pax7^+$ cells in regeneration experiments was normalized to the area of the entire muscle section. Corrected total cell fluorescence (CTCF) was determined for each SC using the calculation:

> Integrated Density − (Area of selected cell × Mean fluorescence of background readings)[45].

RNA isolation and Reverse Transcription

Total RNA was isolated from freshly FACS-isolated or cultured SCs by using the MagMAX 96 total RNA Isolation Kit (Ambion) according to the manufacturer's protocol. The GoScript Reverse Transcription System (Promega) was used for cDNA synthesis from total RNA according to manufacturer's instructions.

Chromatin-Immunoprecipitation (ChIP)

5×10^4–1×10^5 cells were crosslinked in 1% formaldehyde (Thermo Scientific) for 10 min. Crosslinking was quenched with Glycine and cells were washed two times with ice cold PBS. For ChIP of H3K4me3 cells were lysed in Lysis-Buffer (1% SDS, 10mM EDTA, 50mM Tris-HCl pH 8.1, 1× Roche cOmplete Protease Inhibitor) and chromatin was sonicated in Snap Cap microTUBEs using Covaris M220 sonicator to a fragment size of 150

to 300 bp. Chromatin was cleared for 10 min at 17,000 g and 1/10th of chromatin was removed as input fraction. Chromatin was immunoprecipitated overnight with 20 µl Protein A/G bead mix (1:1, Dynabeads®, Invitrogen) pre-coupled with 1 µg antibody (C15410003-50, Diagenode) in ChIP-dilution buffer (0.01% SDS, 1.1% Triton X-100, 1.2mM EDTA, 167mM NaCl, 16.7mM Tris-HCl pH 8.1, 1× Roche Complete Protease Inhibitor). Beads were washed 3 times with Low-Salt buffer (0.1% SDS, 1% Triton X-100, 2mM EDTA, 150mM NaCl, Tris-HCl pH 8.1) and three times with LiCl buffer (350mM LiCl, 1% IPEGAL CA630, 1% deoxycholic acid, 1mM EDTA, 10mM Tris-HCl pH 8.1). For ChIP of Mll1, Wdr5 or HA-tagged Hoxa9 cells were resuspended in Sonication buffer (0.1% SDS, 1% Triton X-100, 0.1% Na-deoxycholate, 1 mM EDTA, 140 mM NaCl, 50 mM Hepes pH 7.9), incubated on ice for 10 min and sonicated to a fragment size of 300 to 600 bp as described above. Chromatin was cleared for 10 min at 17,000 g and unspecific binding was absorbed with 5 µl of Protein G beads for 1 h. 1/10th (Mll1/Wdr5) or 1/20th (HA-tag) of chromatin was removed as input fraction. Chromatin was immunoprecipitated overnight with 2 µg of antibody (Mll1: A300-086A, Wdr5: A302-429A, Bethyl Laboratories; HA-tag: ab9110, Abcam). Chromatin-antibody complexes were captured with 20 µl Protein A/G bead mix (1:1, Dynabeads®, Invitrogen) for 2 h. Beads were washed two times with Sonication buffer, two times with NaCl buffer (0.1% SDS, 1% Triton X-100, 0.1% Na-deoxycholate, 1 mM EDTA, 500 mM NaCl, 50 mM Hepes pH 7.9), two times with LiCl buffer and one time with TE buffer. Decrosslinking and elution was performed in 50 µl Decrosslinking buffer (1% SDS, 100mM $NaHCO_3$, 250mM NaCl) for 4h at 65°C with continuous shaking and subsequent Proteinase K treatment for 1h at 45°C. DNA was purified using Agencourt AMPure XP beads (Beckman Coulter) with a beads:sample ratio of 1.8 or MinElute PCR Purification Kit according to manufacturer's protocols.

Quantitative Real-Time PCR

Quantitative Real-Time PCR (qRT-PCR) was performed with an ABI 7500 Real-Time PCR System (Applied Biosystems) in technical duplicates from the indicated number of biological replicates. The qRT-PCR was carried out in a volume of 12 µl using the Absolute qPCR Rox Mix (Thermo Scientific) and the Universal Probe Library (Roche). Primer and probe sets for the detection of single genes are listed in Table S4. *GAPDH* was detected with Rodent *GAPDH* Control Reagents (Applied Biosystems). Relative expression values were calculated using the ΔCt method.

1. ΔCt = Ct [gene of interest] − Ct [GAPDH]
2. Relative expression = $2(^{-\Delta Ct})$.

qRT-PCR analysis of ChIP samples was performed using SYBR Green Supermix (Biorad) in a final reaction volume of 10 µl and 0.75 µM final primer concentration. Primers are listed in Table S1. HA-tag ChIP signals were calculated as % of the input fraction. The ΔΔCt Method was used to calculate fold enrichment of a genomic locus over the ChIP specific background control (Actb intergenic region for H3K4me3 or gene dessert for Mll1 and Wdr5), both normalized to the signal in the input fraction:

1. ΔCt [normalized to Input] = (Ct [ChIP] – (Ct [Input] – Log2 (Input Dilution Factor))).

2. ΔΔCt = ΔCt [region of choice normalized to Input] – ΔCt [control region normalized to Input].

3. Fold enrichment = $2^{(-\Delta\Delta Ct)}$.

Nanostring analysis

Pellets of freshly isolated SCs were lysed with 3 μl RLT buffer (QIAGEN) and subjected to Nanostring analysis according to manufacturer's instructions using a custom-made *Hox* gene nCounter Elements™ TagSet (Nanostring Technologies). Relative expression to the housekeeping genes *GAPDH*, *Hydroxymethylbilane synthase* (*HMBS*) and *RNA polymerase II subunit A* (*Polr2a*) was calculated using nSolver Software (v2.0) after background correction and normalization to hybridized probe signals.

Proteomic analysis of histone modifications

Preparation of histones for mass spectrometry, data acquisition and analysis was essentially performed as described in 21 with modifications described below. In brief, histones were isolated by acid extraction, derivatised by d6-acetic anhydride (CD3CO, Aldrich) and digested with sequencing-grade trypsin (Promega) over night at a trypsin:protein ratio of 1:20. To acetylate free peptide N-termini, trypsinised histones were derivatised again for 45 minutes at 37°C using 1:20 v/v d6-acetic anhydride (CD3CO, Aldrich) in 50 mM ammonium bicarbonate buffered to pH 8 by ammonium hydroxide solution. After derivatization, peptides were evaporated in a speed-vac at 37°C to near dryness, resuspended in 50 μl of 0.1 formic acid and purified by a StageTip protocol using two discs of C18 followed by one disc of activated carbon (3M Empore). After StageTip purification, the samples were evaporated in a speed-vac to near dryness, resuspended in 20 μl of 0.1% formic acid and stored at −20°C until mass spectrometry acquisition. The histone samples were separated on a reversed-phase liquid chromatography column (75-μm, New Objective) that was packed in-house with a 15-cm stationary phase (ReproSil-Pur C18-AQ, 1.9 μm). The column was connected to a nano-flow HPLC (EASY-nLC 1000; Thermo Scientific) and peptides were electrosprayed in a Q Exactive mass spectrometer (Thermo Fisher Scientific, Waltham, MA, USA). Buffer A was composed of 0.1 % formic acid in HPLC-grade water and buffer B was 0.1 % formic acid in ACN. Peptides were eluted in a linear gradient with a flow rate of 300 nl per minute, starting at 3% B and ramping to 35% in 52 minutes, followed by an increase to 50% B in 4 minutes, followed by an increase to 98% in 4 minutes and then holding at 98% B for another 6 minutes. MS was operated in a combined shotgun-PRM mode targeting positional isomers. Ion chromatograms were extracted with Thermo Xcalibur and Skyline and data summarization and statistical analysis was performed in Excel and R. Relative abundances were calculated from the raw signal reads, according to the formulas described in 21 without further normalisations.

Microarray and bioinformatics analysis

Gene expression analysis was performed using the Mouse GE 8×60K Microarray Kit (Agilent Technologies, Design ID 028005). 100 ng total RNA isolated from SCs were used for the labeling. Samples were labeled with the Low Input Quick Amp Labeling Kit (Agilent Technologies) according to the manufacturer's instructions. Slides were scanned using a

microarray scanner (Agilent Technologies). Expression data were extracted using the Feature Extraction software (Agilent Technologies). Preprocessing of expression data was performed according to Agilent's standard workflow. Using 5 quality flags (gIsPosAndSignif, gIsFeatNonUnifOL, gIsWellAboveBG, gIsSaturated, and gIsFeatPopnOL) from the Feature Extraction software output, probes were labeled as detected, not detected, or compromised. Gene expression levels were background corrected, and signals for duplicated probes were summarized by geometric mean of non-compromised probes. After log2 transformation, a percentile shift normalization at the 75% level and a baseline shift to the median baseline of all probes was performed. All computations were performed using the R statistical software framework (http://www.R-project.org). Differentially expressed genes were calculated by the shrinkage T-statistic[46] and controlled for multiple testing by maintaining a FDR < 0.05[47].

RNA-sequencing analysis

Sequencing reads were filtered out for low quality sequences and trimmed of low quality bases by using FASTX-Toolkit (http://hannonlab.cshl.edu/fastx_toolkit/). Mapping to mm9 genome was performed by using TopHat software[48]. Gene quantification was performed by using HT-Seq and differentially expressed genes (DEGs) were estimated by using DESEQ2[49,50] within the R statistical software framework (http://www.R-project.org) with $p<0.01$. Pearson correlation heatmaps were generated by using custom R scripts by selecting genes having more than 10 read counts in all the samples of at least one condition and an interquartile range (IQR) > 0.5. Significance of overlapping DEGs was calculated by normal approximation of hypergeometric probability.

Identification of Hoxa9 binding sites

Transcription start and end sites of putative Hoxa9 target genes were collected from the UCSC Genome Browser[51] with mm8 track. Sequences in gene body regions (from transcription start to end sites), promoter regions (−2/+1 kb relative to transcription start sites), and distal intergenic regions (−50/+50 kb relative to transcription start sites) of 26 genes were prepared for identification of Hoxa9 binding sites. These sequences were aligned based on the previously reported consensus motifs for Hoxa9-Meis1-Pbx1 (ATGATTTATGGC)[52] and Meis1 (TGTC)[53]. Putative Hoxa9 binding sites were aligned when they contained either no mismatch or one mismatch, and Meis1 motifs were aligned with no mismatch allowed. Hoxa9 binding sites with at least one Meis1 binding site within 300 bp on the same DNA strand were selected for further analysis. Identified Hoxa9 binding sites are listed in Table S5.

Statistics

If not stated otherwise, results are presented as mean with standard error (s.e.m.) from the number of samples indicated in the figure legends. Two groups were compared by two-sided student's t-test or two-sided Mann-Whitney U-test. For multiple comparisons a two-way analysis of variance (ANOVA) was performed using a FDR < 0.5 to correct for multiple comparisons. Statistical significance was set at *, $p<0.05$; **, $p<0.01$; ***, $p<0.001$; ****, $p<0.0001$; with ns, not significant. Statistical analysis was done using GraphPad Prism 6 software and R (v3.3.1).

Extended Data

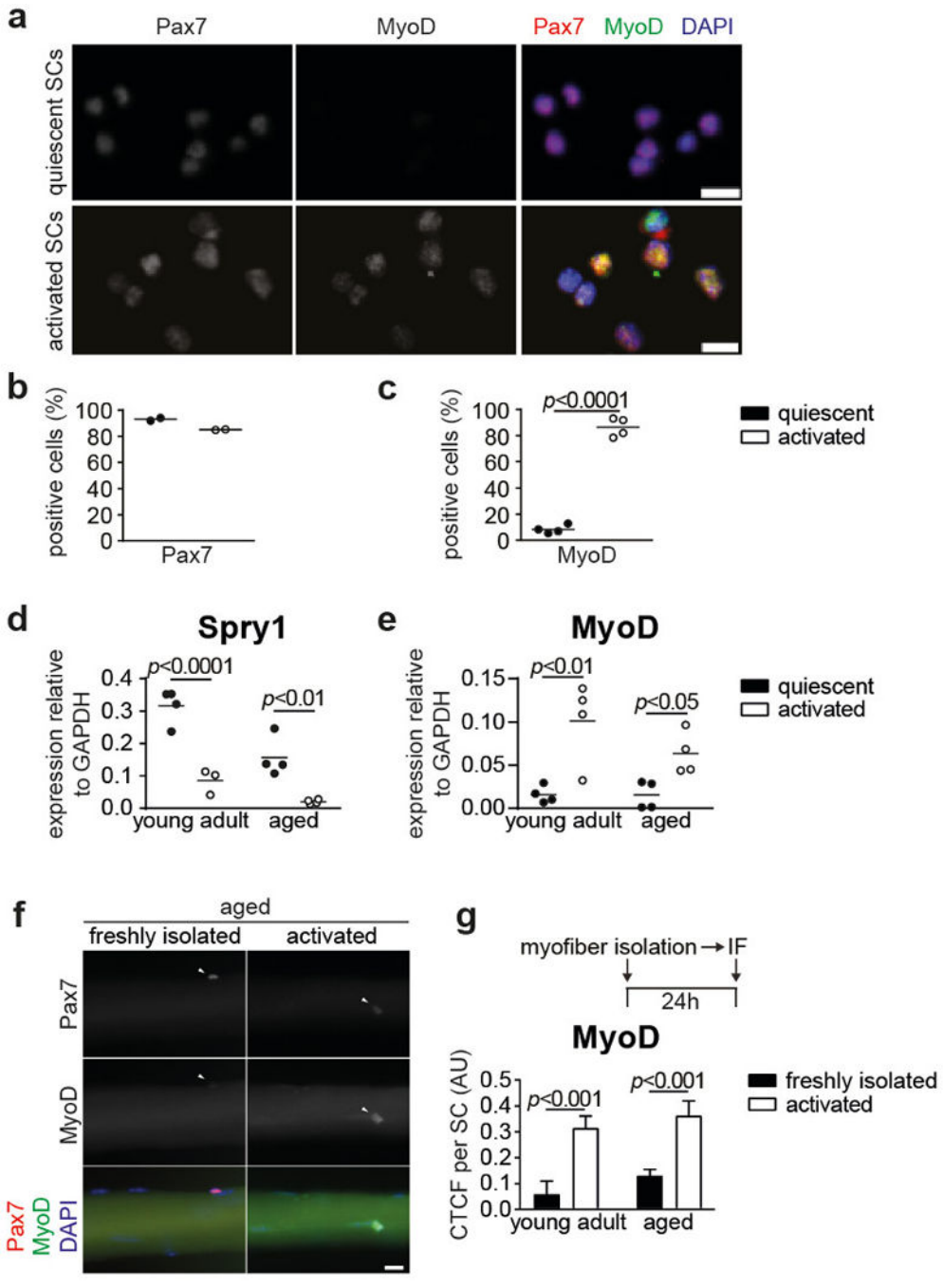

Extended Data Figure 1. SC activation

a, Immunofluorescence (IF) staining for Pax7 and MyoD of freshly isolated SCs from injured (activated SCs) and uninjured muscles (quiescent SCs) from young adult mice. Nuclei were counterstained with DAPI (blue). **b–c**, Quantification of Pax7$^+$ cells (b) and MyoD$^+$ cells (c) in a. **d–e**, qRT-PCR analysis of *Spry1* (d) and *MyoD* (e) expression in freshly isolated quiescent and *in vivo* activated SCs of young adult and aged mice. **f**, IF

staining for Pax7 and MyoD on freshly isolated and 24h cultured myofibers from aged mice. Nuclei were counterstained with DAPI (blue). **g**, CTCF (Corrected total cell fluorescence) for MyoD per SC as in f. Scale bars = 10μm for a; 20 μm for f. Comparisons by two-sided student's t-test (b–c) or two-way ANOVA (d–e, g); n=2 mice for b; n=4 mice for c; n=3 mice (young activated), n=4 mice (all others) for d; n=4 mice for e; n=33/24 nuclei (young), n=35/20 nuclei (aged) from 3 mice for g.

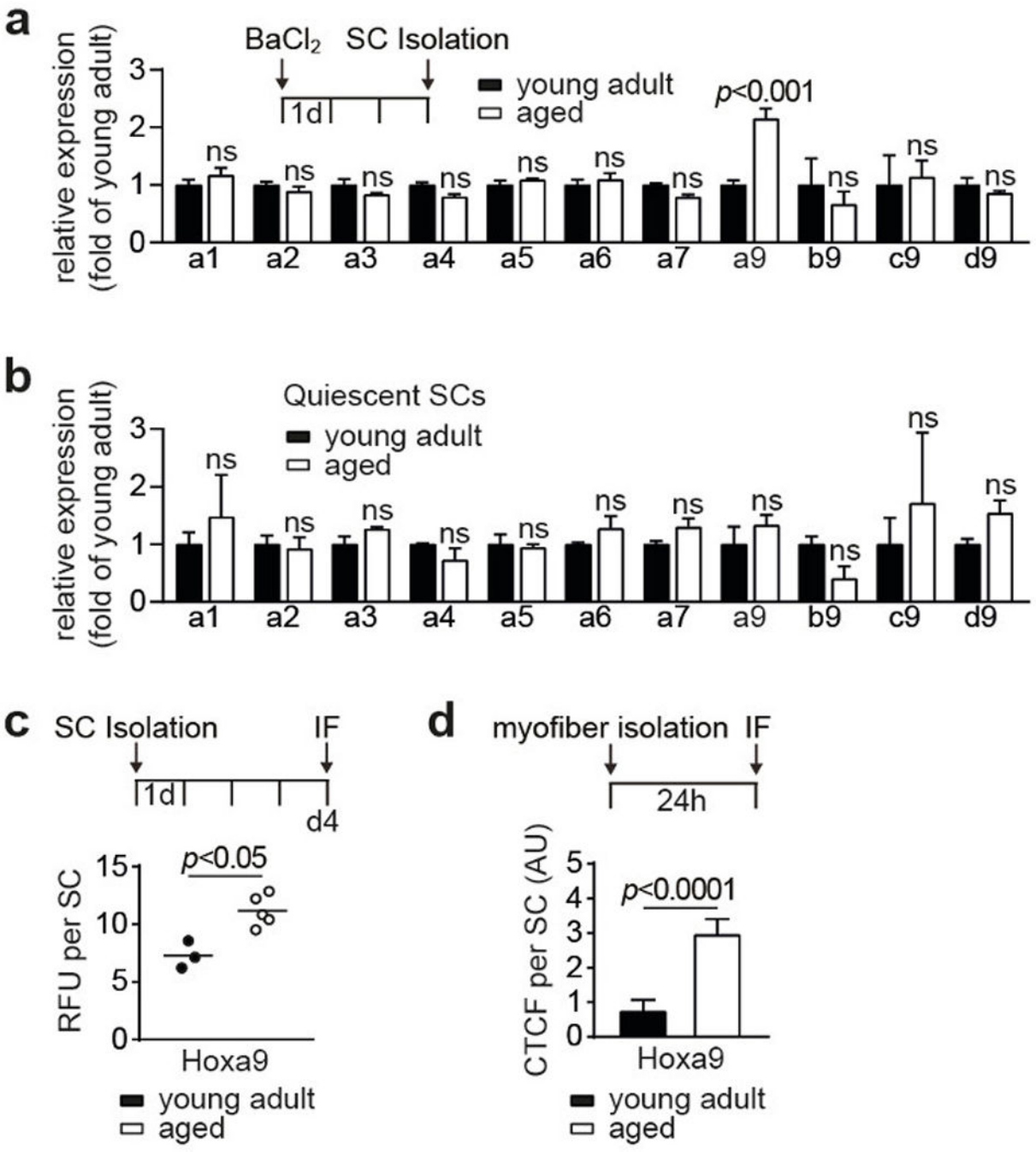

Extended Data Figure 2. Expression of *Hox* genes in SCs

a–b, Nanostring analysis of mRNA expression of *HoxA* genes and *Hoxa9* paralogs (*b9-c9-d9*) in *in vivo* activated (a) and quiescent (b) freshly isolated SCs from young adult and aged mice. **c**, Relative fluorescence units (RFU) for Hoxa9 per SC in 4d cultured SCs from young adult and aged mice. **d**, CTFC for Hoxa9 per activated SC on 24h cultured myofibers as in Fig. 1d. Comparisons by two-way ANOVA (a–b) or two-sided Mann-Whitney U-test (c–d). n=3 mice for a–b; n=3 mice (young), n=5 mice (aged) for c; n=34 nuclei (young), n=32 nuclei (aged) from 4 mice for d.

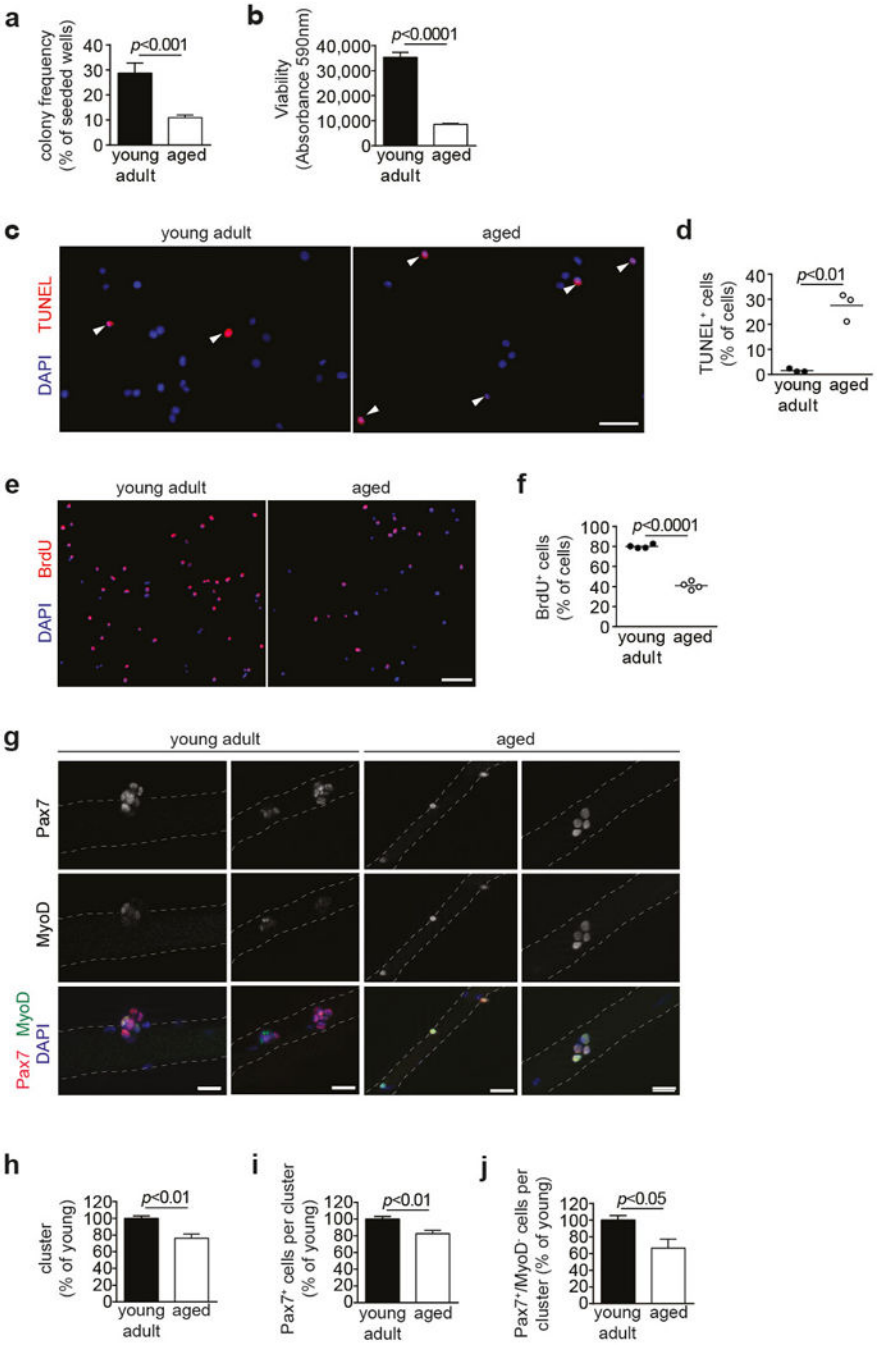

Extended Data Figure 3. Functional decline in aged SCs

a, SCs from young adult and aged mice were sorted as single cells. After 5d, the frequency of myogenic colonies was assessed. The presence of at least 2 cells was considered as colony. **b**, Equal numbers of FACS-isolated SCs from young adult and aged mice were cultured for 4d and Alamar Blue assay was performed. **c**, TUNEL staining of SCs isolated from young adult or aged mice after 4d of culture. Nuclei were counterstained with DAPI (blue). **d**, Quantification of apoptosis based on TUNEL staining in c. **e**, BrdU staining of SCs isolated from young adult or aged mice after 4d of culture. Nuclei were counterstained with DAPI (blue). **f**, Quantification of proliferation based on BrdU staining in e. **g**, IF staining for Pax7 and MyoD on myofibers isolated from young adult and aged mice after 72h in culture. Nuclei were counterstained with DAPI (blue). **h–j**, Quantification of the number of SC-derived clusters with at least 3 adjacent cells (h), average number of all $Pax7^+$ cells (i), or proportion of $Pax7^+/MyoD^-$ cells (j) within clusters as in g. Scale bars = 20 μm for c, g; 50 μm for e. Comparisons by two-sided student's t-test. n=8 mice (young), n=10 mice (aged) for a; n=7 mice (young), n=5 mice (aged) for b; n=3 mice for d; n=4 mice for f; n=4 mice (aged) for j, n=5 mice (all others) for h–j.

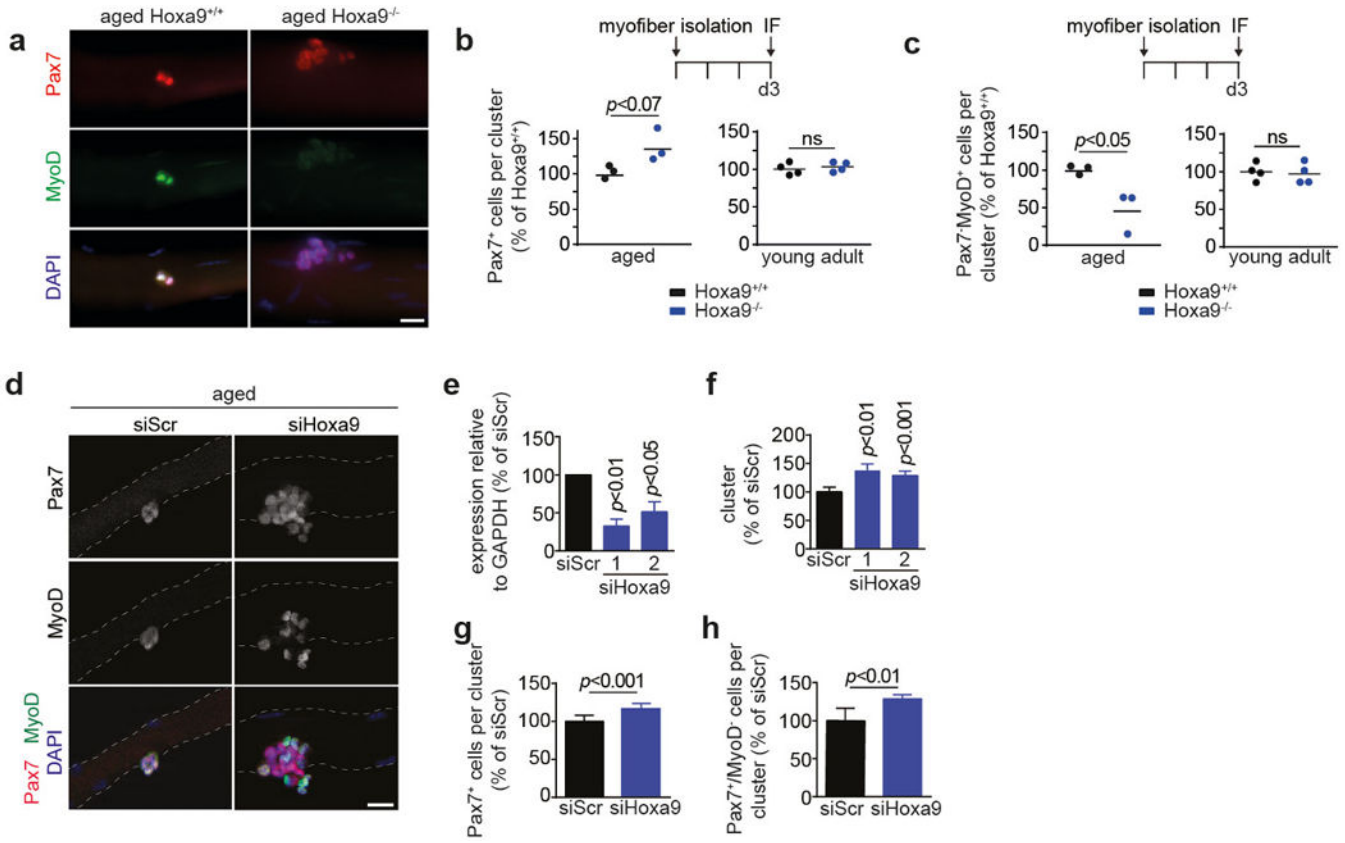

Extended Data Figure 4. Deletion or knockdown of Hoxa9 improves SC function in myofiber cultures

a, IF staining for Pax7 and MyoD on 72h cultured myofiber-associated SCs from aged *Hoxa9*$^{+/+}$ and *Hoxa9*$^{-/-}$ mice. **b–c**, Average number of all $Pax7^+$ cells (b) or $Pax7^-/MyoD^+$ cells (c) within clusters from aged or young adult *Hoxa9*$^{+/+}$ and *Hoxa9*$^{-/-}$ mice as shown in

a. **d**, IF staining for Pax7 and MyoD on 72h cultured myofibers isolated from aged mice transfected with *Hoxa9* or scrambled siRNAs. Nuclei were counterstained with DAPI (blue). **e**, qRT-PCR analysis of *Hoxa9* expression in SCs transfected with *siHoxa9* or siScr. Two *Hoxa9* siRNAs with different target sequences (Supplementary Table 1) were used. **f–h**, Analysis of 72h cultured myofibers from d. Quantification of the number of SC-derived clusters with at least 3 adjacent cells (f), average number of all $Pax7^+$ cells (g), or proportion of $Pax7^+/MyoD^-$ cells (h) within clusters. Scale bars = 20 μm for a, d. Dashed lines outline myofibers. Comparisons by two-sided student's t-test. n=3 mice (aged), n=4 mice (young) for b–c; n=3 mice for e; n=5 mice for f–h.

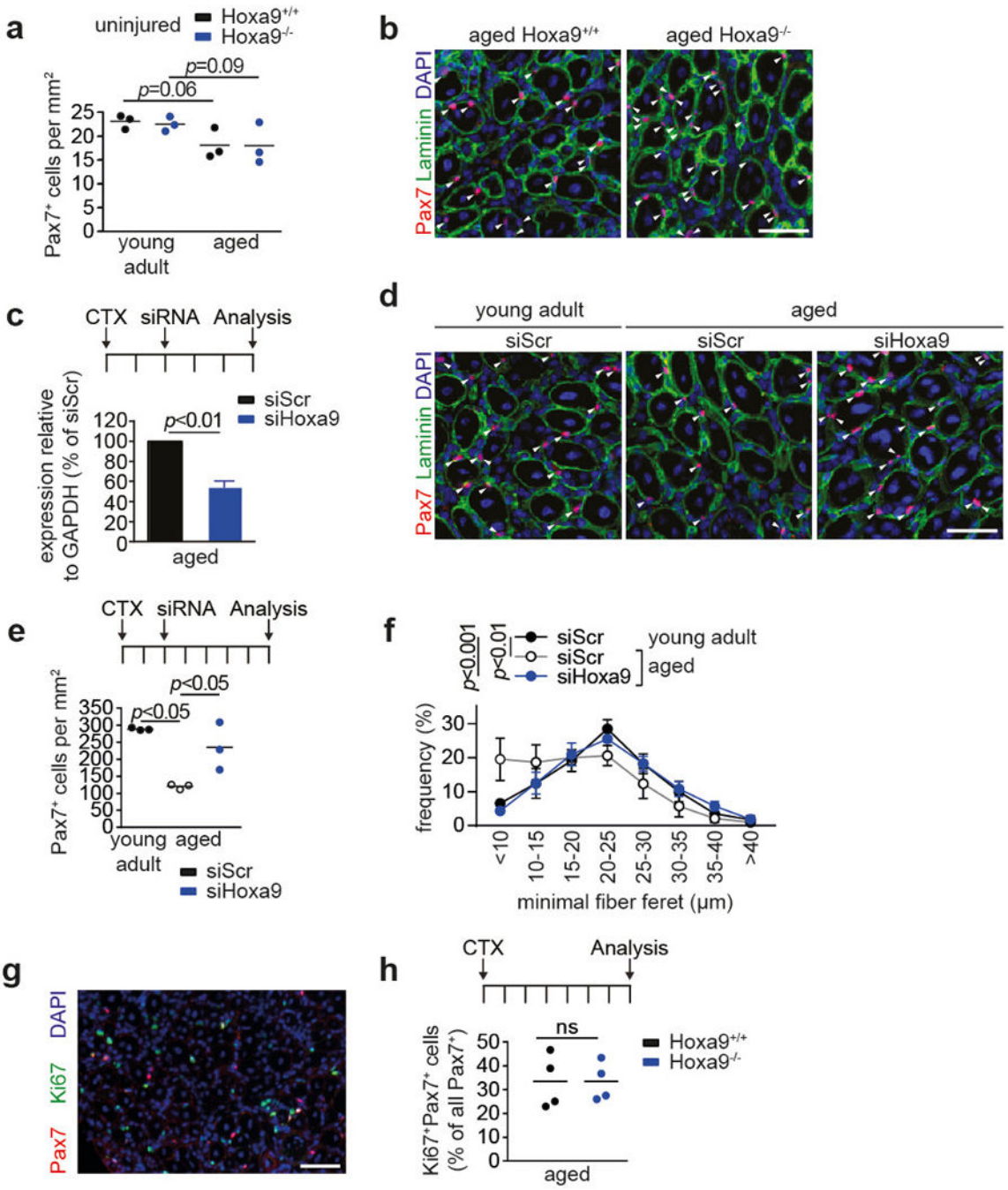

Extended Data Figure 5. Inhibition of *Hoxa9* improves muscle regeneration in aging mice

a, Quantification of Pax7$^+$ cells per area in uninjured tibialis anterior (TA) muscles from young adult and aged *Hoxa9*$^{+/+}$ and *Hoxa9*$^{-/-}$ mice. **b**, IF staining for Pax7 and Laminin on tibialis anterior (TA) muscles from aged *Hoxa9*$^{+/+}$ and *Hoxa9*$^{-/-}$ mice 7d after Cardiotoxin (CTX) injury. **c**, qRT-PCR analysis of *Hoxa9* expression in SCs isolated from TA muscles injected with a self-delivering Hoxa9 or scrambled siRNA and harvested 5d after muscle injury. **d**, IF staining for Pax7 and Laminin of injured TA muscles from young adult and aged mice that were injected with a self-delivery siRNA and harvested 7d after muscle

injury. Nuclei were counterstained with DAPI (blue). Arrowheads denote Pax7$^+$ cells. **e**, Quantification of Pax7$^+$ cells from d per area. **f**, Frequency distribution of minimal fiber feret from d. **g**, IF staining for Pax7 and Ki67 on TA muscles from aged *Hoxa9*$^{+/+}$ and *Hoxa9*$^{-/-}$ mice 7d after muscle injury. Nuclei were counterstained with DAPI (blue). **h**, Quantification of proliferating SCs (Ki67$^+$/Pax7$^+$) as depicted in g. Scale bars = 50 μm for b, d, g. Comparisons by two-sided student's t-test (c, h) or two-way ANOVA (a, e–f). n=3 mice for a; n=3 mice for c; n=3 mice for e–f; n=4 mice for h.

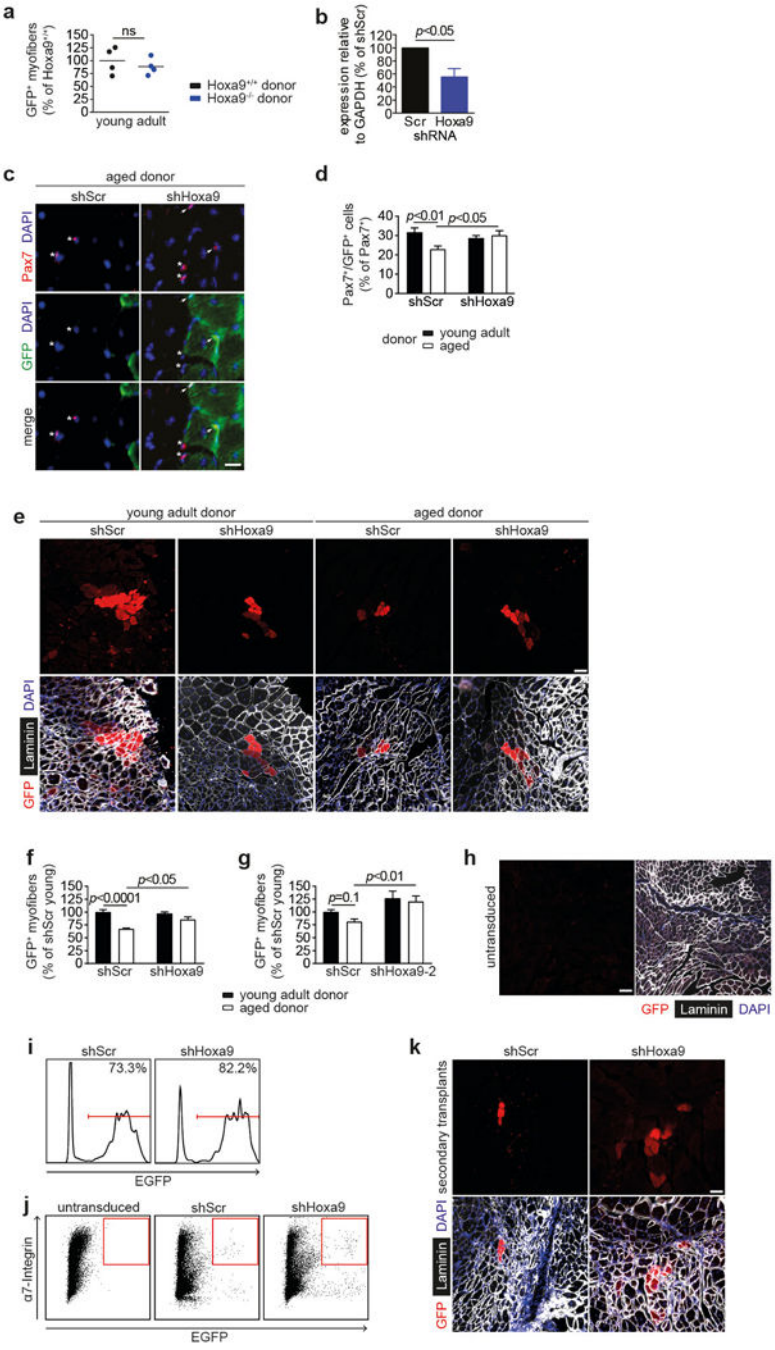

Extended Data Figure 6. Inhibition of *Hoxa9* improves regenerative capacity of aged SCs

a, Quantification of donor-derived (GFP^+) myofibers from transplantation of SCs from young adult *Hoxa9*$^{+/+}$ and *Hoxa9*$^{-/-}$ mice. **b**, qRT-PCR analysis of *Hoxa9* expression in SCs transduced with *shHoxa9* or shScr encoding lentivirus. **c–g**, Transplantation of GFP-labelled SCs from young adult and aged mice that were targeted with an shRNA against Hoxa9 or a scrambled shRNA: (c) IF staining for Pax7 and GFP of transplanted muscle sections. Nuclei were counterstained with DAPI (blue). Arrowheads denote $Pax7^+/GFP^+$ cells, asterisks label $Pax7^+/GFP^-$ cells; (d) Quantification of donor-derived (GFP^+) $Pax7^+$ cells in c; (e) IF staining for GFP and Laminin of transplanted muscle sections, nuclei were counterstained with DAPI (blue); (f–g) Quantification of donor-derived (GFP^+) myofibers in e for two different *Hoxa9* shRNAs in two independent experiments. **h**, IF staining for GFP and Laminin in TA muscles engrafted with untransduced aged SCs. Nuclei were counterstained with DAPI (blue). **i**, Flow-cytometric analysis of transduction efficiency of donor SCs used for transplantation in primary donors analyzed in Fig. 2f. **j**, Representative flow-cytometry plots for re-isolation of transplanted aged SCs that were untransduced as control or transduced with shScr or *shHoxa9* encoding lentivirus as quantified in Fig. 2f. **k**, IF staining for GFP and Laminin in engrafted TA muscles from secondary recipients quantified in Fig. 2g. Nuclei were counterstained with DAPI (blue). Scale bars = 20 μm for c; 50 μm for h; 100 μm for e, k. Comparisons by two-sided student's t-test (a–b) or two-way ANOVA (d, f–g). n=4 recipient mice for a; n=3 mice for b; n=6 recipient mice (young donors), n=4 recipient mice (aged donors) for d, f; n=5 recipient mice for g.

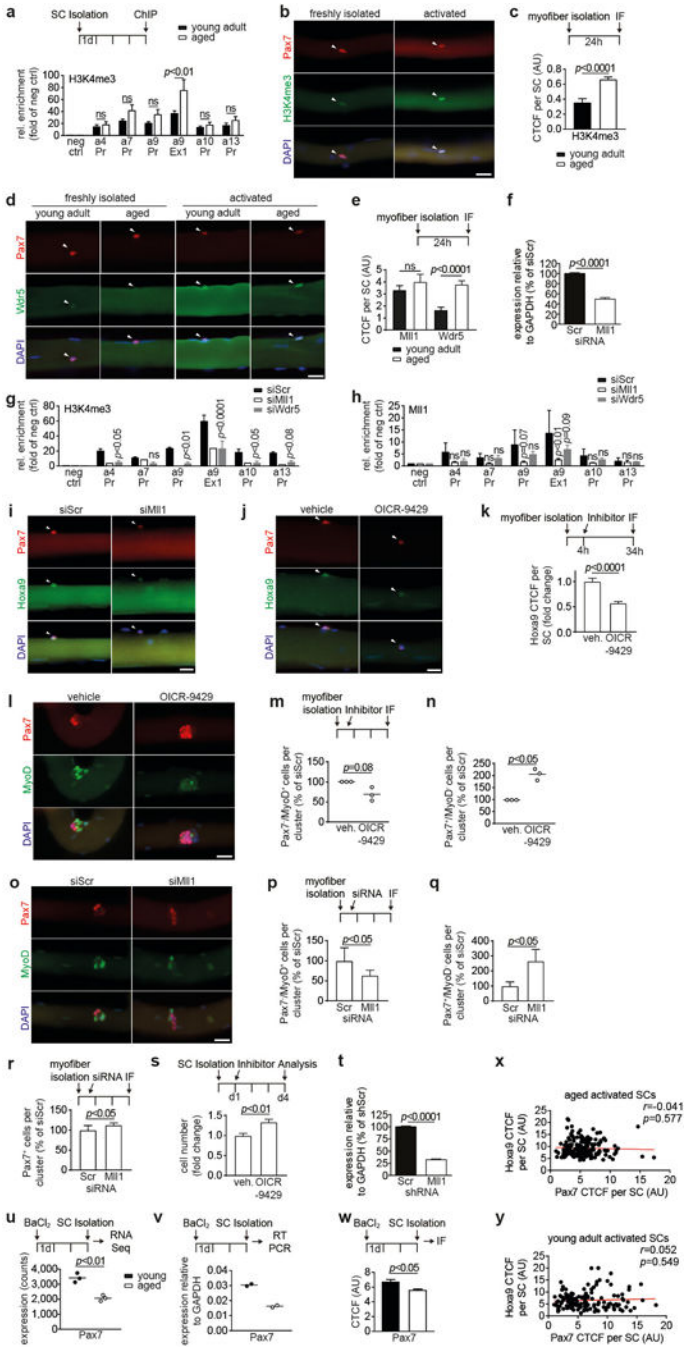

Extended Data Figure 7. Inhibition of Mll1 rescues H3K4me3 induction, *Hoxa9* overexpression, and functional impairment of activated SCs from aged mice

a, ChIP for H3K4me3 at promoters (Pr) or exons (Ex) of indicated *Hox* genes in activated SCs (4d culture) from young adult and aged mice. **b**, IF staining for Pax7 and H3K4me3 on myofiber-associated SCs from aged mice that were freshly isolated or activated by 24h culture of myofibers. **c**, CTCF for H3K4me3 on activated SCs shown in b. **d**, IF staining for Pax7 and Wdr5 on myofiber-associated SCs from young adult aged mice that were freshly isolated or activated by 24h culture of myofibers. **e**, CTCF for Mll1 and Wdr5 per activated

SC as shown in d. **f**, qRT-PCR analysis of Mll1 in SCs transfected with *siMll1* or siScr. **g–h**, ChIPs for H3K4me3 (g) and Mll1 (h) in primary myoblasts 3d after transfection with the indicated siRNAs. **i–j**, IF staining for Pax7 and Hoxa9 in myofibers from aged mice after transfection with *siMll1* or siScr (i, quantification in Fig. 3d) or after treatment with OICR-9429 or vehicle (j). **k**, CTCF for Hoxa9 per SC in j. **l**, IF staining for Pax7 and MyoD on OICR-9429 treated myofibers from aged mice after 72h culture. Nuclei were counterstained with DAPI (blue). **m–n**, Average number of $Pax7^{-}/MyoD^{+}$ cells (m) or $Pax7^{+}/MyoD^{-}$ cells (n) within clusters in l. **o**, IF staining for Pax7 and MyoD on siRNA treated myofibers from aged mice after 72h culture. Nuclei were counterstained with DAPI (blue). **p–r**, Average number of $Pax7^{-}/MyoD^{+}$ cells (m), $Pax7^{+}/MyoD^{-}$ cells (n) or $Pax7^{+}$ cells (r) within clusters in o. **s**, Relative changes in cell number of aged SCs after treatment with OICR-9429 and 4d culture, compared to vehicle control. **t**, qRT-PCR analysis of Mll1 in SCs transduced with *shMll1* or shScr. **u–w**, Analysis of Pax7 expression in *in vivo* activated SCs from young adult and aged mice by RNA-sequencing (u), qRT-PCR (v), or IF depicted in Fig. 1b (w). **x-y**, Pearson correlation comparing the Hoxa9 IF signal (Quantification in Fig. 1c) and the Pax7 IF signal (Quantification in Extended Data Fig. 7w) of activated SCs from aged (x) and young adult (y) mice. Note, there is no correlation between Hoxa9 expression level and Pax7 expression level in activated SCs from aged mice. Scale bars = 20 μm for b, d, i–j, l, o. Comparisons by two-way ANOVA (a, g–h), two-sided student's t-test (f, m–n, p–v), two-sided Mann-Whitney U-test (c, e, k, w) or Pearson correlation (x-y). n=4 mice (young), n=7 mice (aged) for a; n=27 nuclei from 2 mice (young), n=27 nuclei from 4 mice (aged) for c; n=40/52 nuclei (Mll1), n=44/99 nuclei (Wdr5) from 3 young/aged mice for e; n=3 mice for f; n=3 biological replicates (siWdr5), n=2 biological replicates (siMll1) for g; n=3 biological replicates for h; n=173 nuclei (DMSO), n=324 nuclei (OICR-9429) from 4 mice for k; n=3 mice for m–n; n=7 mice for p–r; n=6 mice for s; n=3 mice for t; n=3 mice for u; n=2 mice for v; n=134 nuclei (young), n=181 nuclei (aged) from 3 mice for w–y.

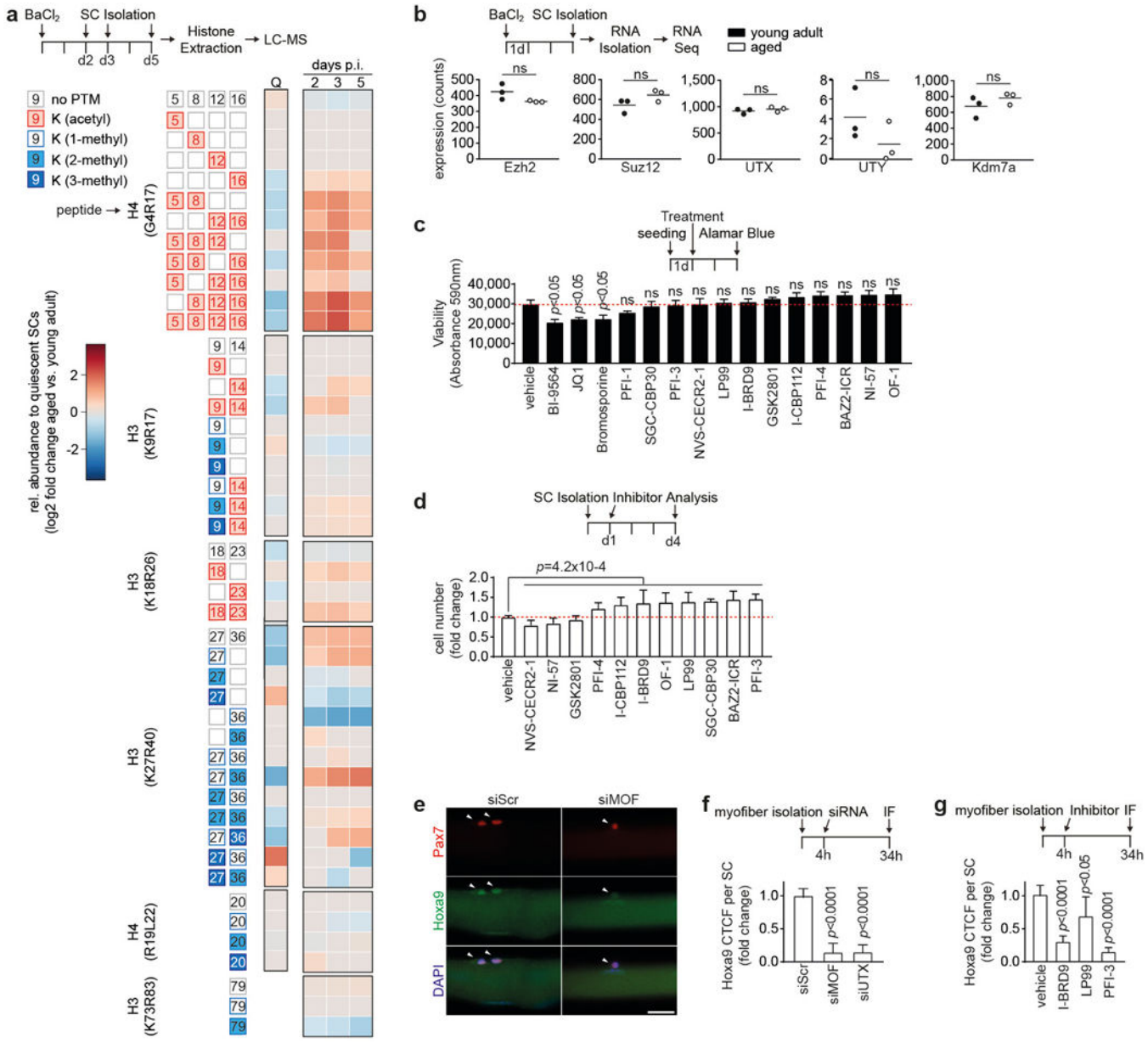

Extended Data Figure 8. Alterations in the epigenetic stress response of activated SCs from aged mice

a, Heatmap displaying relative changes in abundance of different histone modifications in freshly isolated SCs from aged compared to young adult mice. SCs were analyzed in quiescence (Q, derived from uninjured muscle) or at the indicated time points after activation mediated by muscle injury. Relative abundances at indicated days after injury (days p.i.) are first normalized on quiescent SCs, and then compared between SCs isolated from aged and young adult mice and log2 scaled. Only significant changes are shown (p<0.05). **b**, Expression analysis of the indicated genes in freshly isolated *in vivo* activated SCs from young adult and aged mice based on RNA-sequencing. **c**, Viability of primary myoblasts after 48h treatment with Bromodomain Inhibitors (1μM) from the Structural Genomics Consortium Probe Set, measured by Alamar Blue assay. **d**, Relative changes in

cell number of aged SCs after treatment with non-toxic Bromodomain Inhibitors (1μM) from c and 4d culture, compared to vehicle control. A Wilcoxon rank sum test on the ratio of all cell counts being equal to 1 was performed to test the hypothesis of a general effect of the inhibitors on cell number. **e**, IF staining for Pax7 and Hoxa9 in siRNA treated myofiber-associated SCs from aged mice. **f**, CTCF for Hoxa9 per SC in e. **g**, Quantification of IF staining for Hoxa9 in $Pax7^{+}$ cells on myofiber-associated SCs from aged mice treated with Bromodomain inhibitors. Scale bars = 20 μm for e. Comparisons by two-sided student's t-test (a–c), Wilcoxon rank sum test (d) or two-sided Mann-Whitney U-test (f–g). n=4 mice for a; n=3 mice for b; n=4 biological replicates for c; n=6 mice for d; n=71 nuclei (siScr), n=48 nuclei (siMOF), n=98 nuclei (siUTX) from 3 mice for f; n=60 nuclei (vehicle), n=59 nuclei (I-BRD9), n=38 nuclei (LP99), n=62 nuclei (PFI-3) from 3 mice for g.

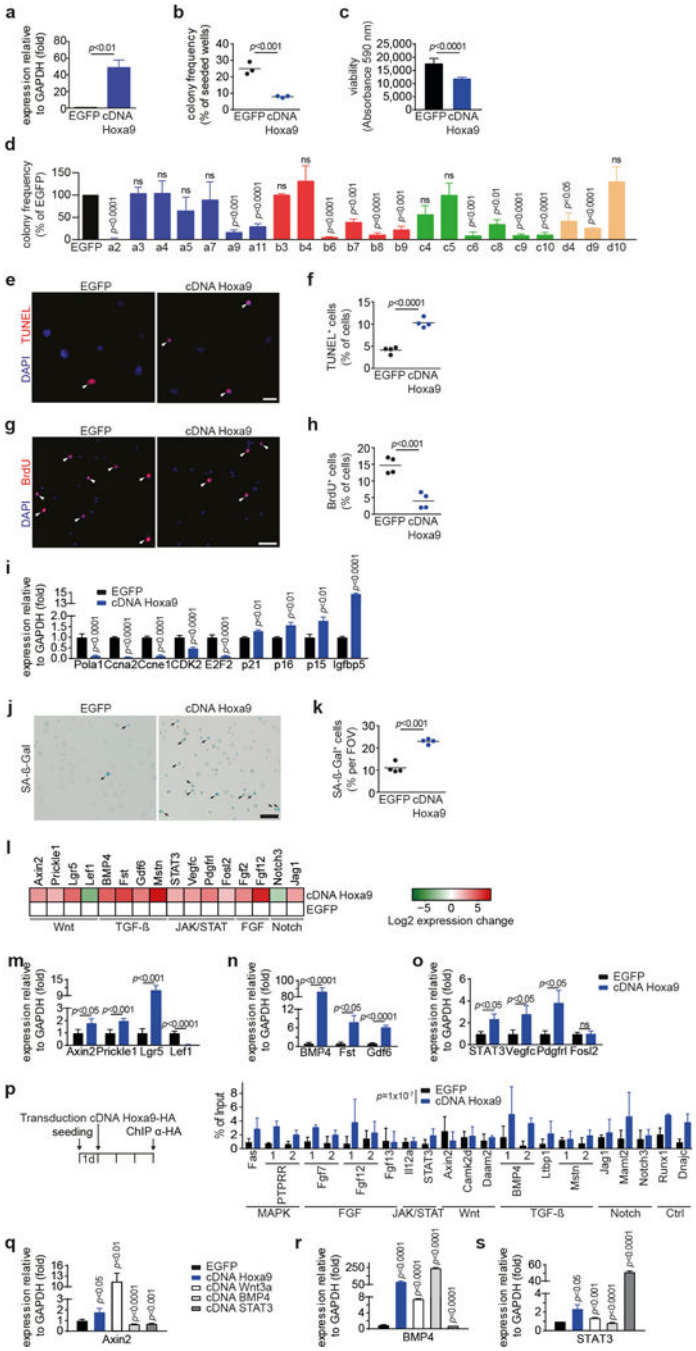

Extended Data Figure 9. Overexpression of *Hox* genes inhibits SC function

a, Expression of *Hoxa9* in SCs transduced with *Hoxa9* cDNA or EGFP as control. **b–c**, FACS-isolated SCs from young adult mice were transduced with a lentivirus either containing both EGFP and *Hoxa9* cDNA or only EGFP. Infected ($EGFP^+$) cells were isolated after 3 days. (b) Frequency of myogenic colonies from single cell-sorted SCs. (c) Quantification of cell number based on Alamar Blue assay of bulk cultures. **d**, Frequency of myogenic colonies of SCs overexpressing the indicated *Hox* genes. **e+g**, TUNEL (e) or BrdU (g) staining of SCs overexpressing *Hoxa9* or EGFP. Infected (EGFP+) cells were

isolated 3d after transduction and analyzed 3d later. Nuclei were counterstained with DAPI (blue). Arrowheads mark TUNEL or BrdU positive cells. **f+h**, Quantification of apoptosis (f) or proliferation (h) based on TUNEL or BrdU staining as in e or g. **i**, qRT-PCR based expression analysis of various cell-cycle and senescence markers in SCs overexpressing *Hoxa9* compared to EGFP-infected controls, day 5 after infection. **j**, SA-ß-Galactosidase staining of SCs overexpressing *Hoxa9* or EGFP at day 5 after infection. Arrowheads mark SA-ß-Gal positive cells. **k**, Quantification of senescence per field of view (FOV) based on SA-ß-Gal staining in j. **l**, Heat map displaying log2 fold changes of expression of selected genes from microarray analysis in Fig. 5a. **m–o**, qRT-PCR validation of differentially expressed genes annotated to Wnt- (m), TGFß- (n) and JAK/STAT pathways (o) as in l. **p**, Identification of Hoxa9 binding sites by anti-HA ChIP of primary myoblasts overexpressing HA-tagged *Hoxa9* cDNA or EGFP as control. Shown is the qRT-PCR for 1 or 2 putative Hoxa9 binding sites at the indicated loci. Hoxa9 binding sites at target genes were identified as described in Methods and are listed in Supplementary Table 1. A two-sided block bootstrap test on the difference of the percentage of bound DNA for all binding sites being equal to 0 was performed to test the hypothesis of a generally increased binding Hoxa9. **q–s**, SCs were infected with lentiviruses expressing *Hoxa9*, *Wnt3a*, *BMP4*, *STAT3* cDNAs or EGFP. qRT-PCR analysis of expression of the indicated target genes at 5 days after infection: Axin2 (q), BMP4 (r) and STAT3 (s). Scale bars = 20 μm for e, g, 50 μm for j. Comparisons by two-sided student's t-test (a–d, f, h, k, q–s) or two-way ANOVA (i, m–o). n=4 mice for a; n=3 mice for b; n=7 mice for c; n=3 mice for d; n=4 mice for f, h, k; n=3 mice (p15, p21), n=6 mice (p16), n=4 mice (all others) for i; n=4 pools of 3 mice for l; n=4 mice for m–o; n=3 biological replicates for p; n=3 mice (Wnt3a, BMP4, STAT3), n=4 mice (EGFP, Hoxa9) for q–s.

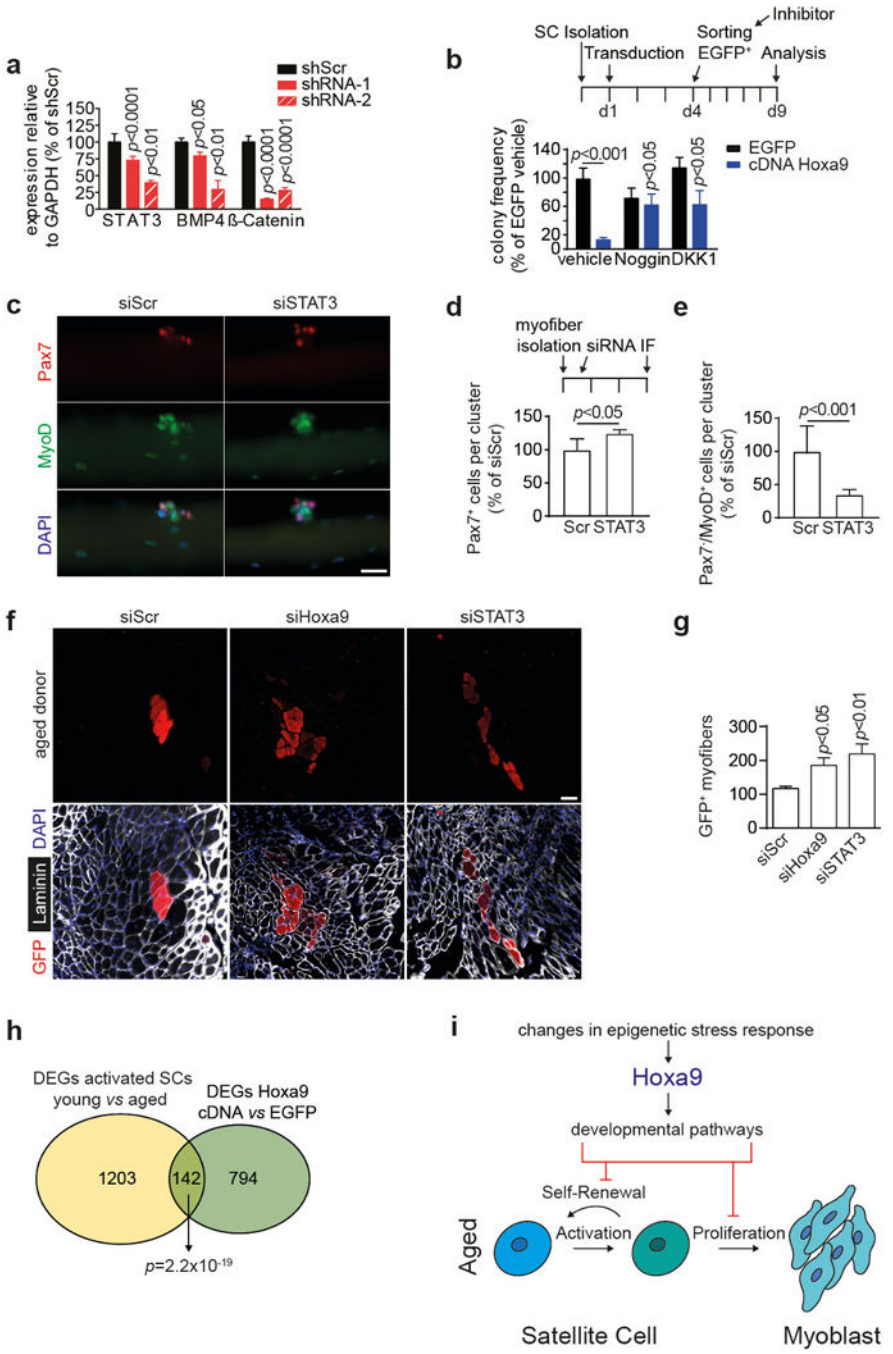

Extended Data Figure 10. Validation of Hoxa9 downstream targets

a, Knockdown efficiency of two shRNAs (red bars) for *STAT3*, *BMP4* and *ß-Catenin*. **b**, SCs from young adult mice were transduced with a *Hoxa9* and EGFP encoding lentivirus. EGFP^{+} cells were sorted as single cells and cultured in the presence of Noggin, DKK1 or PBS/0.1% BSA as vehicle. Colony frequency was assessed after 5d and is compared to *Hoxa9* cDNA expressing cells treated with vehicle control. **c**, IF staining for Pax7 and MyoD on siRNA transfected myofibers from aged mice after 72h culture. Nuclei were counterstained with DAPI (blue). **d–e**, Average number of Pax7^{+} cells (d) or Pax7^{-}/MyoD^{+}

cells (e) within clusters in c. **f**, IF staining for GFP and Laminin in TA muscles engrafted with siRNA transfected SCs isolated from GFP transgenic aged mice. Nuclei were counterstained with DAPI (blue). **g**, Quantification of donor-derived (GFP^+) myofibers in f. **h**, Area-proportional Venn diagram of differentially expressed genes (DEGs) from indicated transcriptomes. **i**, Model for the Hoxa9-mediated impairment of SC function during aging: quiescent SCs become activated upon muscle injury and proliferate as myoblasts to repair damaged muscle tissue. After activation. aged SCs display global and locus-specific alterations in the epigenetic stress response resulting in overexpression of *Hoxa9*, which in turn induces developmental pathways inhibiting SC function and muscle regeneration in aged mice. Scale bars = 20 μm for c, 100 μm for f. Comparisons by two-way ANOVA (a–b) or two-sided student's t-test (d–e, g). n=3 mice for a; n=4 mice for b; n=5 mice for d–e; n=5 recipient mice for g; n=3 mice per group (activated SCs), n=4 pools of 3 mice (Hoxa9 overexpression) for h.

Supplementary Material

Refer to Web version on PubMed Central for supplementary material.

Acknowledgments

We thank Y. Morita and A. Illing for providing guidance regarding FACS analysis. We are thankful to the FLI Core Facilities Functional Genomics (T. Kroll, A. Ploubidou) and DNA Sequencing (M. Groth) for their services. We express our thanks to M. Burkhalter, T. Sperka and A. Illing for constructive discussions and suggestions. We are grateful to B. Wollscheid and S. Goetze for providing support for proteomic measurements. We thank V. Sakk and M. Kettering for mouse husbandry as well as S. Eichwald, K. Tramm and A. Abou Seif for experimental assistance. We are grateful to M. Kessel, M. Kyba, G. Sauvageau and D. Wellik for sharing plasmids with *Hox* cDNAs. We thank the Structural Genomics Consortium and S. Ackloo for providing access to the epigenetic probe library. We further thank M. Cerletti for providing protocols on SC isolation and E. Perdiguero for advice on infection of SCs prior to transplantation. Work on this project in KLR's laboratory was supported by the DGF (RU-745/10, RU-745/12), the ERC (2012-AdG 323136), the state of Thuringia, and intramural funds from the Leibniz association. J.V.M. was supported by a grant from the DFG (MA-3975/2-1). C.F. acknowledges support by the DFG (FE-1544/1-1) and EMBO (long-term postdoctoral fellowship ALTF 55-2015). R.A. was supported by the ERC (AdvGr 670821 (Proteomics 4D)). The funding for the $Hoxa9^{-/-}$ mice to K.L.M. was provided by a grant of the NIH (HL096108). R.R. was supported by a grant from the NIH (R01GM106056). This work was further supported by grants to H.A.K. from the DFG (SFB 1074 project Z1), the BMBF (Gerontosys II, Forschungskern SySTaR, project ID 0315894A), and the European Community's Seventh Framework Programme 390 (FP7/2007-2013, grant agreement n○602783).

References

1. Rando TA. Stem cells, ageing and the quest for immortality. Nature. 2006; 441:1080–1086. DOI: 10.1038/nature04958 [PubMed: 16810243]
2. Brack AS, et al. Increased Wnt signaling during aging alters muscle stem cell fate and increases fibrosis. Science. 2007; 317:807–810. DOI: 10.1126/science.1144090 [PubMed: 17690295]
3. Carlson ME, et al. Relative roles of TGF-beta1 and Wnt in the systemic regulation and aging of satellite cell responses. Aging cell. 2009; 8:676–689. DOI: 10.1111/j.1474-9726.2009.00517.x [PubMed: 19732043]
4. Sousa-Victor P, et al. Geriatric muscle stem cells switch reversible quiescence into senescence. Nature. 2014; 506:316–321. DOI: 10.1038/nature13013 [PubMed: 24522534]
5. Conboy IM, Conboy MJ, Smythe GM, Rando TA. Notch-mediated restoration of regenerative potential to aged muscle. Science. 2003; 302:1575–1577. DOI: 10.1126/science.1087573 [PubMed: 14645852]
6. Price FD, et al. Inhibition of JAK-STAT signaling stimulates adult satellite cell function. Nature medicine. 2014; 20:1174–1181. DOI: 10.1038/nm.3655

7. Krumlauf R. Hox genes in vertebrate development. Cell. 1994; 78:191–201. [PubMed: 7913880]
8. Lawrence HJ, Sauvageau G, Humphries RK, Largman C. The role of HOX homeobox genes in normal and leukemic hematopoiesis. Stem cells. 1996; 14:281–291. DOI: 10.1002/stem.140281 [PubMed: 8724694]
9. Cosgrove BD, et al. Rejuvenation of the muscle stem cell population restores strength to injured aged muscles. Nature medicine. 2014; 20:255–264. DOI: 10.1038/nm.3464
10. Artavanis-Tsakonas S, Rand MD, Lake RJ. Notch signaling: cell fate control and signal integration in development. Science. 1999; 284:770–776. [PubMed: 10221902]
11. Lyons KM, Pelton RW, Hogan BL. Organogenesis and pattern formation in the mouse: RNA distribution patterns suggest a role for bone morphogenetic protein-2A (BMP-2A). Development. 1990; 109:833–844. [PubMed: 2226202]
12. Munoz-Espin D, et al. Programmed cell senescence during mammalian embryonic development. Cell. 2013; 155:1104–1118. DOI: 10.1016/j.cell.2013.10.019 [PubMed: 24238962]
13. Sehgal, PB., Levy, DE., Hirano, T. Signal transducers and activators of transcription (STATs) : activation and biology. Kluwer Academic; 2003.
14. Sinha M, et al. Restoring systemic GDF11 levels reverses age-related dysfunction in mouse skeletal muscle. Science. 2014; 344:649–652. DOI: 10.1126/science.1251152 [PubMed: 24797481]
15. Bernet JD, et al. p38 MAPK signaling underlies a cell-autonomous loss of stem cell self-renewal in skeletal muscle of aged mice. Nature medicine. 2014; 20:265–271. DOI: 10.1038/nm.3465
16. Soshnikova N, Duboule D. Epigenetic temporal control of mouse Hox genes in vivo. Science. 2009; 324:1320–1323. DOI: 10.1126/science.1171468 [PubMed: 19498168]
17. Ayton PM, Cleary ML. Transformation of myeloid progenitors by MLL oncoproteins is dependent on Hoxa7 and Hoxa9. Genes Dev. 2003; 17:2298–2307. DOI: 10.1101/gad.1111603 [PubMed: 12952893]
18. Yu BD, Hess JL, Horning SE, Brown GA, Korsmeyer SJ. Altered Hox expression and segmental identity in Mll-mutant mice. Nature. 1995; 378:505–508. DOI: 10.1038/378505a0 [PubMed: 7477409]
19. Grebien F, et al. Pharmacological targeting of the Wdr5-MLL interaction in C/EBPalpha N-terminal leukemia. Nature chemical biology. 2015; 11:571–578. DOI: 10.1038/nchembio.1859 [PubMed: 26167872]
20. McKinnell IW, et al. Pax7 activates myogenic genes by recruitment of a histone methyltransferase complex. Nature cell biology. 2008; 10:77–84. DOI: 10.1038/ncb1671 [PubMed: 18066051]
21. Feller C, Forne I, Imhof A, Becker PB. Global and specific responses of the histone acetylome to systematic perturbation. Molecular cell. 2015; 57:559–571. DOI: 10.1016/j.molcel.2014.12.008 [PubMed: 25578876]
22. Liu L, et al. Chromatin modifications as determinants of muscle stem cell quiescence and chronological aging. Cell Rep. 2013; 4:189–204. DOI: 10.1016/j.celrep.2013.05.043 [PubMed: 23810552]
23. Filippakopoulos P, et al. Histone recognition and large-scale structural analysis of the human bromodomain family. Cell. 2012; 149:214–231. DOI: 10.1016/j.cell.2012.02.013 [PubMed: 22464331]
24. Tierney MT, et al. STAT3 signaling controls satellite cell expansion and skeletal muscle repair. Nature medicine. 2014; 20:1182–1186. DOI: 10.1038/nm.3656
25. Chakkalakal JV, Jones KM, Basson MA, Brack AS. The aged niche disrupts muscle stem cell quiescence. Nature. 2012; 490:355–360. DOI: 10.1038/nature11438 [PubMed: 23023126]
26. Blagosklonny MV. Aging is not programmed: genetic pseudo-program is a shadow of developmental growth. Cell cycle. 2013; 12:3736–3742. DOI: 10.4161/cc.27188 [PubMed: 24240128]
27. Martin N, Beach D, Gil J. Ageing as developmental decay: insights from p16(INK4a.). Trends Mol Med. 2014; 20:667–674. DOI: 10.1016/j.molmed.2014.09.008 [PubMed: 25277993]
28. Lawrence HJ, et al. Mice bearing a targeted interruption of the homeobox gene HOXA9 have defects in myeloid, erythroid, and lymphoid hematopoiesis. Blood. 1997; 89:1922–1930. [PubMed: 9058712]

29. Brown PJ, Muller S. Open access chemical probes for epigenetic targets. Future medicinal chemistry. 2015; 7:1901–1917. DOI: 10.4155/fmc.15.127 [PubMed: 26397018]
30. Barsyte-Lovejoy D, et al. Chemical Biology Approaches for Characterization of Epigenetic Regulators. Methods in enzymology. 2016; 574:79–103. DOI: 10.1016/bs.mie.2016.01.011 [PubMed: 27423858]
31. Theodoulou NH, et al. Discovery of I-BRD9, a Selective Cell Active Chemical Probe for Bromodomain Containing Protein 9 Inhibition. Journal of medicinal chemistry. 2016; 59:1425–1439. DOI: 10.1021/acs.jmedchem.5b00256 [PubMed: 25856009]
32. Picaud S, et al. Generation of a Selective Small Molecule Inhibitor of the CBP/p300 Bromodomain for Leukemia Therapy. Cancer research. 2015; 75:5106–5119. DOI: 10.1158/0008-5472.CAN-15-0236 [PubMed: 26552700]
33. Picaud S, et al. PFI-1, a highly selective protein interaction inhibitor, targeting BET Bromodomains. Cancer research. 2013; 73:3336–3346. DOI: 10.1158/0008-5472.CAN-12-3292 [PubMed: 23576556]
34. Martin LJ, et al. Structure-Based Design of an in Vivo Active Selective BRD9 Inhibitor. Journal of medicinal chemistry. 2016; 59:4462–4475. DOI: 10.1021/acs.jmedchem.5b01865 [PubMed: 26914985]
35. Hay DA, et al. Discovery and optimization of small-molecule ligands for the CBP/p300 bromodomains. Journal of the American Chemical Society. 2014; 136:9308–9319. DOI: 10.1021/ja412434f [PubMed: 24946055]
36. Drouin L, et al. Structure enabled design of BAZ2-ICR, a chemical probe targeting the bromodomains of BAZ2A and BAZ2B. Journal of medicinal chemistry. 2015; 58:2553–2559. DOI: 10.1021/jm501963e [PubMed: 25719566]
37. Clark PG, et al. LP99: Discovery and Synthesis of the First Selective BRD7/9 Bromodomain Inhibitor. Angewandte Chemie. 2015; 54:6217–6221. DOI: 10.1002/anie.201501394 [PubMed: 25864491]
38. Chen P, et al. Discovery and Characterization of GSK2801, a Selective Chemical Probe for the Bromodomains BAZ2A and BAZ2B. Journal of medicinal chemistry. 2016; 59:1410–1424. DOI: 10.1021/acs.jmedchem.5b00209 [PubMed: 25799074]
39. Filippakopoulos P, et al. Selective inhibition of BET bromodomains. Nature. 2010; 468:1067–1073. DOI: 10.1038/nature09504 [PubMed: 20871596]
40. Pasut A, Jones AE, Rudnicki MA. Isolation and Culture of Individual Myofibers and their Satellite Cells from Adult Skeletal Muscle. Jove-Journal of Visualized Experiments. 2013
41. Bentzinger CF, et al. Fibronectin regulates Wnt7a signaling and satellite cell expansion. Cell stem cell. 2013; 12:75–87. DOI: 10.1016/j.stem.2012.09.015 [PubMed: 23290138]
42. Schambach A, et al. Lentiviral vectors pseudotyped with murine ecotropic envelope: increased biosafety and convenience in preclinical research. Exp Hematol. 2006; 34:588–592. DOI: 10.1016/j.exphem.2006.02.005 [PubMed: 16647564]
43. Wang J, et al. A differentiation checkpoint limits hematopoietic stem cell self-renewal in response to DNA damage. Cell. 2012; 148:1001–1014. DOI: 10.1016/j.cell.2012.01.040 [PubMed: 22385964]
44. Chambeyron S, Bickmore WA. Chromatin decondensation and nuclear reorganization of the HoxB locus upon induction of transcription. Genes Dev. 2004; 18:1119–1130. DOI: 10.1101/gad.292104 [PubMed: 15155579]
45. Burgess A, et al. Loss of human Greatwall results in G2 arrest and multiple mitotic defects due to deregulation of the cyclin B-Cdc2/PP2A balance. Proceedings of the National Academy of Sciences of the United States of America. 2010; 107:12564–12569. DOI: 10.1073/pnas.0914191107 [PubMed: 20538976]
46. Opgen-Rhein R, Strimmer K. Accurate ranking of differentially expressed genes by a distribution-free shrinkage approach. Stat Appl Genet Mol Biol. 2007; 6 Article9.
47. Benjamini Y, Hochberg Y. Controlling the false discovery rate: a practical and powerful approach to multiple testing. Journal of the Royal Statistical Society. 1995; 57:12.
48. Trapnell C, Pachter L, Salzberg SL. TopHat: discovering splice junctions with RNA-Seq. Bioinformatics. 2009; 25:1105–1111. DOI: 10.1093/bioinformatics/btp120 [PubMed: 19289445]

49. Anders S, Pyl PT, Huber W. HTSeq–a Python framework to work with high-throughput sequencing data. Bioinformatics. 2015; 31:166–169. DOI: 10.1093/bioinformatics/btu638 [PubMed: 25260700]

50. Love MI, Huber W, Anders S. Moderated estimation of fold change and dispersion for RNA-seq data with DESeq2. Genome biology. 2014; 15:550. [PubMed: 25516281]

51. Karolchik D, et al. The UCSC Table Browser data retrieval tool. Nucleic acids research. 2004; 32:D493–496. DOI: 10.1093/nar/gkh103 [PubMed: 14681465]

52. Shen WF, et al. HOXA9 forms triple complexes with PBX2 and MEIS1 in myeloid cells. Molecular and cellular biology. 1999; 19:3051–3061. [PubMed: 10082572]

53. Huang Y, et al. Identification and characterization of Hoxa9 binding sites in hematopoietic cells. Blood. 2012; 119:388–398. DOI: 10.1182/blood-2011-03-341081 [PubMed: 22072553]

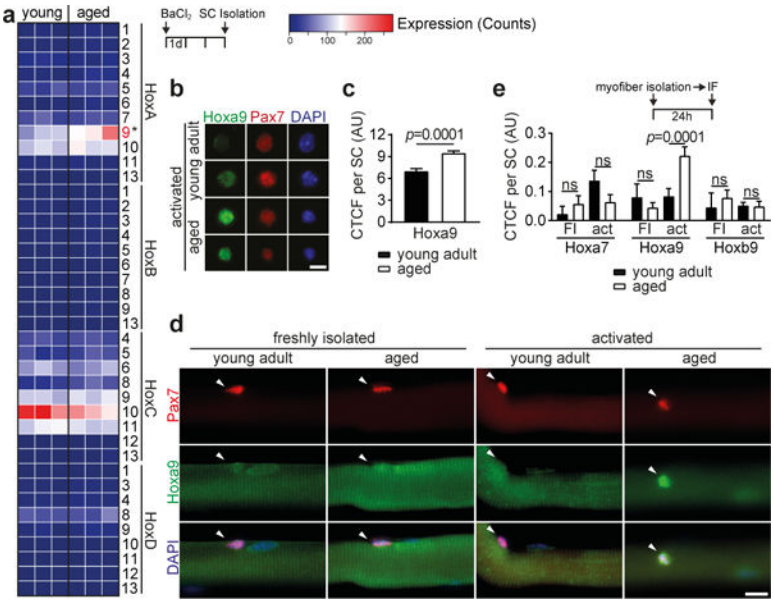

Figure 1. Upregulation of *Hoxa9* in aged activated SCs

a–c, Analysis of freshly isolated, *in vivo* activated SCs (3d after muscle injury with $BaCl_2$) from young adult and aged mice: (a) heatmap showing the mRNA expression of all *Hox* genes as determined by RNA-sequencing analysis; (b) representative picture of immunofluorescence (IF) staining for Hoxa9, Pax7 and DAPI; (c) corrected total cell fluorescence (CTCF) for Hoxa9 per SC as shown in b. AU = arbitrary units. **d,e**, IF staining for Hoxa9 and Pax7 in myofiber-associated SCs that were quiescent (freshly isolated myofibers = FI) or activated (24h culture of myofibers = act): (d) representative pictures with arrowheads denoting $Pax7^+$ cells; (e) CTCF for indicated *Hox* genes. Note the specific induction of Hoxa9 in activated SCs isolated from aged mice. Scale bars = 5 μm for b; 20 μm for d. Comparisons by two-sided Mann-Whitney U-test (c) or two-way ANOVA (e). * = $p<0.05$. n=3 mice for a; n=134 nuclei (young), n=181 nuclei (aged) from 3 mice for c; n=12/13/17/56 nuclei (Hoxa7), n=9/42/102/62 nuclei (Hoxa9), n=7/35/34/25 nuclei (Hoxb9) from 2 young and 4 aged mice for e.

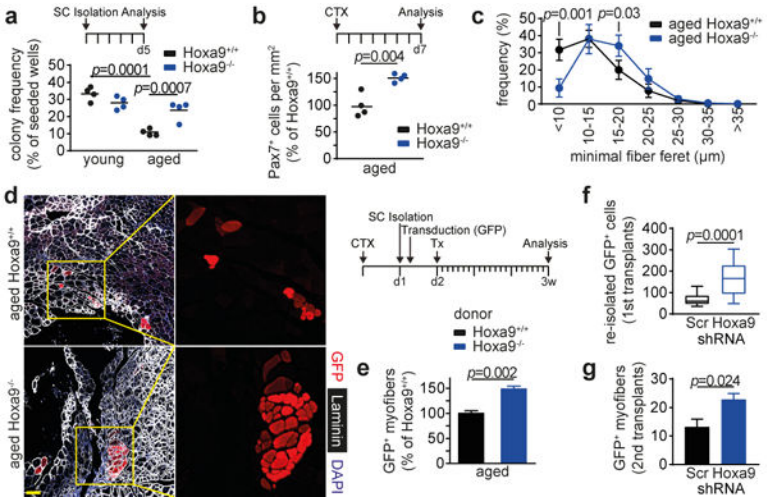

Figure 2. *Hoxa9* deficiency improves muscle regeneration in aged mice

a, Frequency of myogenic colonies derived from single-cell sorted SCs from young adult or aged *Hoxa9*$^{+/+}$ and *Hoxa9*$^{-/-}$ mice after 5d culture. **b,c**, Quantification of Pax7^{+} cells per area (b) and frequency distribution of minimal fiber feret (c) on tibialis anterior (TA) muscles from aged *Hoxa9*$^{+/+}$ and *Hoxa9*$^{-/-}$ mice, 7d after muscle injury with Cardiotoxin (CTX). **d,e**, Transplantation (Tx) of GFP-labelled SCs from aged *Hoxa9*$^{+/+}$ and *Hoxa9*$^{-/-}$ mice: (d) IF staining for GFP, Laminin and DAPI in engrafted TA muscles; (e) quantification of donor-derived (GFP^{+}) myofibers in d. **f**, Quantification of donor-derived (GFP^{+}) SCs re-isolated from primary recipients. **g**, Quantification of donor-derived (GFP^{+}) myofibers from secondary recipients. Scale bars = 50 µm for d. Data in f represent median with 50% confidence interval box and 95% confidence interval whiskers. Comparisons by two-way ANOVA (a, c), two-sided student's t-test (b, e, g) or two-sided Mann-Whitney U-test (f). n=4 mice for a; n=4 mice for b-c; n=8 recipient mice for e; n=20 recipient mice for f; n=5 recipient mice for g.

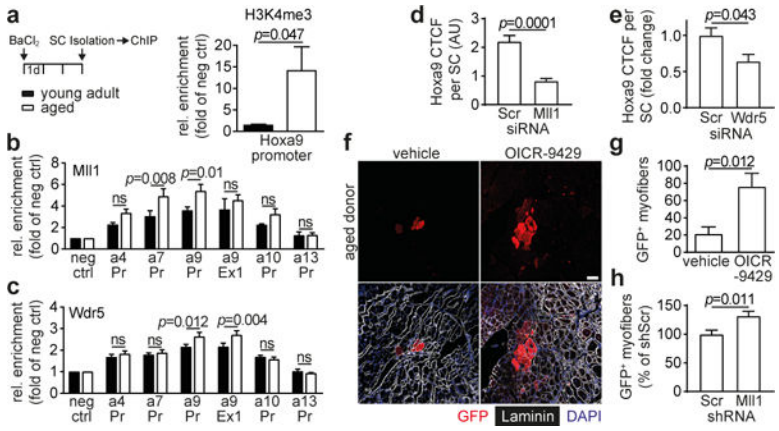

Figure 3. Mll1 complex-dependent chromatin modification induces *Hoxa9* and limits muscle regeneration in aging mice

a–c, Chromatin immunoprecipitation (ChIP)-qPCR analysis of the indicated promoters (Pr) and exons (Ex) in activated SCs from young adult and aged mice using antibodies against H3K4me3 (a), Mll1 (b), or Wdr5 (c). **d,e**, CTCF for Hoxa9 per SC after *siMll1* (d) or *siWdr5* transfection (e) of freshly isolated myofiber-associated SCs from aged mice. **f-h**, Transplantation (Tx) of GFP-labelled SCs from aged mice: (f) representative picture of IF staining for GFP, Laminin and DAPI in engrafted TA muscles after Tx of OICR-9429 treated SCs; quantification of donor-derived (GFP^+) myofibers after Tx of OICR-9429 (g) or shRNA (h) treated SCs. Scale bars = 50 μm for f. Comparisons by two-way ANOVA (b-c), two-sided student's t-test (a, g-h) or two-sided Mann-Whitney U-test (d-e). n=6 mice for a; n=7 mice (young), n=10 mice (aged) for b-c; n=109 nuclei (siScr), n=110 nuclei (siMll1) from 3 mice for d; n=116 nuclei (siScr), n=65 nuclei (siWdr5) from 3 mice for e; n=5 recipient mice for g; n=6 recipient mice for h.

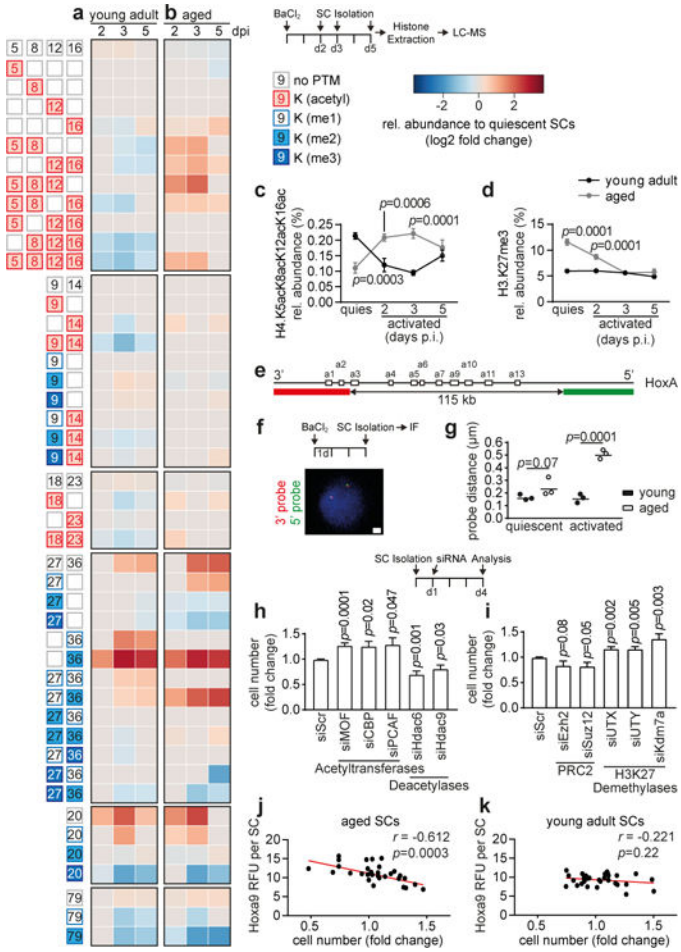

Figure 4. Altered epigenetic stress response in aged satellite cells

a,b, Heatmap of mass-spectrometry (MS) analysis displaying significant (p<0.05) relative changes in abundance of the indicated histone modifications at the indicated days post injury (dpi). **c,d**, Trajectory time-course plots showing relative abundance of H4.K5acK8acK12acK16ac (c) or H3.K27me3 (d) in freshly isolated quiescent (quies) or *in vivo* activated SCs purified at indicated time points post muscle injury (p.i.). **e-g**, Fluorescence *in situ* hybridization of freshly isolated quiescent or *in vivo* activated SCs with the indicated probes (e) spanning the *HoxA* cluster; (f) exemplary image; (g) average probe distance. **h,i**, Relative changes in SC number 4 days after transfection of freshly isolated SCs from aged mice with the indicated siRNAs. **j,k**, Pearson correlation of relative cell number and Hoxa9 immunofluorescence signal of SCs from young adult and aged mice 4d after transfection with a selection of siRNAs targeting different classes of chromatin modifiers. RFU = Relative fluorescence units. Scale bars = 1 µm for f. Comparisons by two-way ANOVA (c-d, g), two-sided student's t-test (a-b, h-i), or Pearson correlation (j-k). n=4 mice for a-d; n=3 mice with 50 nuclei per replicate for g; n=7 mice (Ezh2), 8 mice (all others) for h-i; n=6 mice (aged), n=3 mice (young) for j-k.

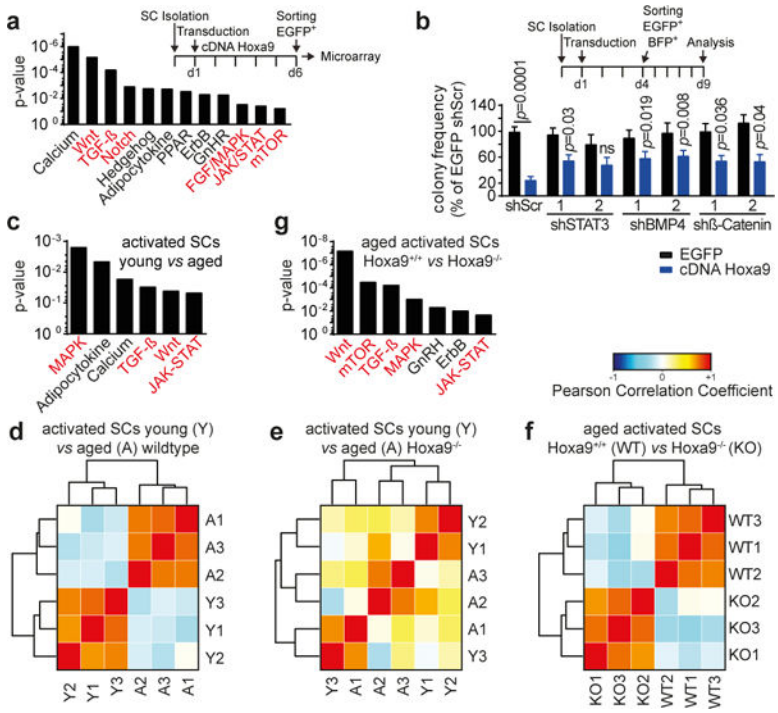

Figure 5. Activation of *Hoxa9* induces developmental pathways

a–b, KEGG analysis of differentially expressed genes (DEGs) of SCs overexpressing *Hoxa9* compared to EGFP. Red-highlighted pathways were previously shown to impair the function of SCs in aging mice. **b**, Colony formation of single cell-sorted, *Hoxa9*-overexpressing SCs derived from young adult mice that were co-infected with the indicated shRNAs together with indicated shRNAs; comparison to *Hoxa9*/shScr co-infected cells. **c,g**, KEGG analysis of DEGs from indicated transcriptomes. **d-f**, Heatmaps displaying Pearson correlation analysis of indicated transcriptomes. Comparisons by two-way ANOVA (c). n=4 pools of 3 mice for a; n=6 mice (shSTAT3-2), n=7 mice (all others) for b; n=3 mice per group for c–f.